Chapter 3:

Biochemical and structural characterisation of monofunctional *Plasmodium falciparum* AdoMetDC

3.1. Introduction

Targeting of AdoMetDC activity has previously been shown to be effective in antiparasitic strategies such as *T. b. brucei*-infected rats. Treatment of the infected rats with MDL73811 resulted in a 20-fold increase in AdoMet levels [175]. In addition, DFMO treatment of trypanosomes isolated from these infected rats also resulted in a 50-fold increase in AdoMet levels. In the latter study a massive >4 000-fold increase in dcAdoMet levels was also observed since putrescine as acceptor of the aminopropyl moiety from dcAdoMet was depleted upon inhibition of ODC activity with DFMO [176]. These results showed that inhibition of *T. brucei* AdoMetDC with MDL73811 leads to a trypanosome-specific increase in AdoMet, which could be responsible for the trypanosomal-specific hypermethylation of nucleic acids and/or proteins via the inhibition of the polyamine biosynthesis pathway [175-177]. Histone and DNA methylation has transcriptional regulatory effects [178,179] and hypermethylation may result in the down-regulation of transcription [180].

In *P. falciparum*, MDL73811 has also been shown to irreversibly inhibit *Pf*AdoMetDC activity resulting in the prevention of parasite growth *in vitro* [115] and resulted in the prevention of hypusine formation for eIF-5A synthesis [181]. In contrast to the observed effect in trypanosomes, metabolomic studies have shown that, while co-inhibition of *Pf*AdoMetDC and *Pf*ODC with MDL73811 and DFMO causes cytostasis, inhibition does not alter AdoMet levels, possibly due to the observed down-regulation of AdoMet synthetase [116]. However, another study has shown that plasmodial AdoMet synthase is not allosterically regulated by AdoMet [93], which indicates that a different mechanism exists for the homeostatic control of AdoMet levels within *P. falciparum* to prevent hypermethylation. The polyamine pathway in the plasmodial parasite therefore seems to be highly regulated in order to link methionine metabolism with that of polyamine levels. Further investigations are needed to identify possible allosteric effector/s of the bifunctional *Pf*AdoMetDC/ODC activities, while the bifunctional arrangement in itself could allow for the simultaneous regulation of both activities exerted by the effector/s.

Extensive studies on the bifunctional *Pf*AdoMetDC/ODC protein provided important insights into several biochemical properties of the bifunctional protein such as its oligomeric arrangement as a heterotetramer, obligate homodimer formation of *Pf*ODC, effects of putrescine on *Pf*ODC and *Pf*AdoMetDC activities, the role of the hinge region and *Pf*AdoMetDC domain in *Pf*ODC activity, the presence and functional roles of parasite-specific inserts and the effects of various inhibitors on enzyme activities [69-71,100,103]. Homology models have also been solved for both monofunctional domains, which provided important insights into the active sites as well as inhibitor binding to *Pf*ODC [120,127]. Apart from the predictions obtained from the *Pf*AdoMetDC homology model, comparatively few studies have been performed on this monofunctional *Pf*AdoMetDC domain and aspects such as its functional oligomeric status, the details of its mechanism of autocatalytic processing, role as a partner protein to *Pf*ODC and regulator of enzyme activities within the bifunctional complex remains to be identified. In context of the well-studied *Pf*ODC domain [103] and the proposed role of the bifunctional *Pf*AdoMetDC/ODC arrangement in mediating the decarboxylase domain activities as identified in Chapter 2, the *Pf*AdoMetDC domain should be investigated to determine its biochemical properties as well as its role within the bifunctional complex. These results could provide novel insights into the observed differences in parasite responses upon treatment with polyamine biosynthesis inhibitors as well as possibilities to improve the mainly cytostatic effect observed with DFMO and MDL73811 treatment [118,182].

Previous studies of *Pf*AdoMetDC in either its monofunctional or bifunctional form showed that the *Pf*AdoMetDC active site can function independently while the optimal activity of *Pf*ODC is dependent on the presence of the hinge region as well as the *Pf*AdoMetDC domain [71,103]. A follow-up study showed that interdomain interactions within the bifunctional complex are mediated by parasite-specific inserts [69]. Recently, it was shown that trypanosomal AdoMetDC is activated by a catalytically inactive AdoMetDC homologue, or prozyme [163,164] while human ODC is inhibited by the presence of antizyme [128]. In contrast to the human and trypanosomal proteins, *Pf*AdoMetDC activity and autocatalytic processing is not stimulated by putrescine [71], making this enzyme a comparatively less catalytic efficient enzyme and indicates that an as of yet unidentified effector could mediate the kinetic properties of this enzyme. As mentioned previously it has been speculated that the bifunctional arrangement in *P. falciparum* could allow for the simultaneous regulation of both the domains within the *Pf*AdoMetDC/ODC complex [71], which is similar to the domains within the *Pf*DHFR/TS bifunctional protein [122].

The crystal structures of various AdoMetDC and ODC proteins have been solved, which provided insights into several aspects concerning protein function, regulation and druggability. For AdoMetDC, the structures of human, plant (*S. tuberosum*) and prokaryotic (*T. maritima*) AdoMetDCs have been determined [123,183,184]. The quaternary structure of the active, human AdoMetDC revealed a four-layer αββα-sandwich fold, which at the time of publishing, had not been observed in any other protein structure in the Protein Data Bank [123]. It has previously been suggested that AdoMetDC might be a product of an ancient gene duplication event that resulted in its structural similarity [184]. The protein exists as an $(\alpha\beta)_2$ dimer where the α- and β-subunits are formed by an autocatalytic processing event (non-hydrolytic serinolysis) that takes place at hSer68 (human residue Ser68), which simultaneously results in the formation of the active site pyruvoyl co-factor. The mechanism of processing has been studied in human and *T. cruzi* AdoMetDC and the specific residues involved in the autocatalytic reaction have been characterised [125,185-189]. Several human AdoMetDC crystal structures of unprocessed mutants or a protein locked as an ester intermediate have been solved, which provided novel insights into the autocatalytic reaction mechanism. Each (αβ) monomer contains two central eight-stranded β-sheets that are flanked by several α- and 3_{10}-helices on either side. The two monomers are then joined by an edge-on association of the β-sheets at the dimer interface to form the dimeric protein. The active sites of the monomers are located between the α- and β-subunits of each monomer where the pyruvoyl group is formed and is thus located distant from the dimer interface. An unusual collection of charged residues between the β-sheets of each monomer, well-removed from the active site, has been shown as the site where the positively-charged putrescine binds. The crystal structure of plant AdoMetDC showed that the protein adopts the same αββα-fold as the dimeric human protein but revealed two major differences, namely: 1) plant AdoMetDC is constitutively active since putrescine does not stimulate autocatalytic processing nor catalytic activity; and 2) plant AdoMetDC exists as a monomeric protein. Even though plant AdoMetDC also contains most of the charged-buried residues present in the human putrescine-binding site, three positively-charged residues and several water molecules were shown to mimic putrescine binding [184,189].

The homology model of *Pf*AdoMetDC with the plant and human structures as templates showed that the protein also adopts the same αβ-fold as seen for the template AdoMetDCs [120]. The model has an equal number of strands as in the human template but differences exist in the number of α- and 3_{10}-helices flanking the β-sheets of the αββα-fold. Like plant AdoMetDC, *Pf*AdoMetDC activity is not affected by putrescine nor does it require putrescine for the

autocatalytic processing reaction [71]. In the absence of putrescine these proteins may be constitutively active to allow for continuous supply of product, which is nonsensical in the case of the plant AdoMetDC due to the various essential functions that the polyamines mediate while *Pf*AdoMetDC activity may be regulated by a different mechanism. As mentioned earlier, the inhibition of *Pf*AdoMetDC does not lead to accumulation of AdoMet, nor would dcAdoMet be synthesised if it is not required by the parasite since dcAdoMet is exclusively used as a substrate in the polyamine pathway [178], thus once produced it is committed to this pathway. Furthermore, previous studies have shown that within the bifunctional complex, the *Pf*ODC domain affects the kinetic properties of *Pf*AdoMetDC [71]. Therefore, instead of the product of the ODC reaction stimulating *Pf*AdoMetDC activity, the entire protein may conformationally contribute to mediate catalytic activity. Activity analyses of the monofunctional and bifunctional forms of *Pf*AdoMetDC showed an increase in substrate affinity from 58 µM to 43 µM, respectively, while the specific activities remained similar (as recalculated in nmol/min per mol protein) [71].

In this chapter, the expression and purification of soluble, monofunctional *Pf*AdoMetDC within *E. coli* was improved, which allowed investigations of various biochemical and structural aspects of this protein such as enzyme kinetics and oligomeric status. Comparisons could subsequently be drawn with trypanosomal and human AdoMetDCs in terms of the oligomeric status, secondary structure and the mechanism of autocatalytic processing of the *Pf*AdoMetDC protein. The results obtained in this study support previous studies that were performed on the *Pf*ODC domain, which suggested that the unique arrangement of *Pf*AdoMetDC and *Pf*ODC in the bifunctional complex allows for the concurrent regulation of the enzyme activities and could provide a possible explanation for the absence of *Pf*AdoMetDC stimulation by putrescine.

3.2. Methods

3.2.1. Cloning of the harmonised *PfAdometdc* gene sequence

Codon harmonisation was carried out in an attempt to improve the heterologous expression of the *Pf*AdoMetDC domain within *E. coli* with the use of a web interface algorithm (http://www.sami.org.za/equalize/). Nucleotides 1 to 1461 were replaced by synonymous codons that ensured the positional codon frequency of low/intermediate and high usage codons to remain similar to the frequency used by that of the *E. coli* host [190]. This region corresponds to approximately the first third of the entire bifunctional *PfAdometdc/Odc* gene and encodes for the

487-residue catalytic domain of *Pf*AdoMetDC (Figure 3.1A and B).

Custom gene synthesis was performed by GeneArt, (Regensburg, Germany) and the shipping plasmid containing the harmonised insert was received in dried form. The plasmid was dissolved and then transformed into electrocompetent *E. coli* SURE cells (Stratagene). Transformed cells were selected for ampicillin resistance on LB-agar plates and grown overnight at 37°C. A single colony was picked and inoculated for 16 h at 30°C in LB-ampicillin (50 µg/ml) for subsequent plasmid purification. The shipped and the pASK-IBA3 plasmids containing the wild-type, unharmonised *PfAdometdc/Odc* insert (Figure 3.1A, pASK-IBA3 *A/Owt*) [70] were both digested with *Xba*I and *Kpn*I (Promega) at 37°C for 1 h in order to replace the corresponding wild-type, unharmonised *PfAdometdc* sequence with the harmonised *PfAdometdc* insert from the shipping plasmid with restriction enzyme-mediated cloning (Figure 3.1C). The bands corresponding to the 1461 bp harmonised insert and the 5911 bp pASK-IBA3 *A/Owt* fragment (with wild-type unharmonised *PfAdometdc* removed) were excised and purified from an agarose gel and ligated at 4°C for 48 h using T4 DNA Ligase (Promega). The ligated, circular product was then transformed into electrocompetent *E. coli* SURE cells. Colonies were picked for plasmid extraction and verified with restriction mapping.

However, since the exact C-terminal end of the *Pf*AdoMetDC domain within *Pf*AdoMetDC/ODC is unclear, a harmonised fragment was created that included 255 wild-type, unharmonised nucleotides at the C-terminus of the gene encoding the catalytic domain of *PfAdometdc* (Figure 3.1E). This fragment was amplified from the construct containing the partially harmonised *PfAdometdc/Odc* sequence described above (Figure 3.1C). The length of this 572-residue protein was based on the portion used for the *Pf*AdoMetDC homology model, which consisted of 526 residues [128] with a buffer of 45 residues since the extent of the *Pf*AdoMetDC domain is unknown. A second construct was also created that included 519 wild-type, unharmonised nucleotides (Figure 3.1F, total of 1980 nucleotides) in order to mimic the size of the published monofunctional *Pf*AdoMetDC domain (Figure 3.1D, wt*Pf*AdoMetDC-hinge) and includes half of the hinge region [78].

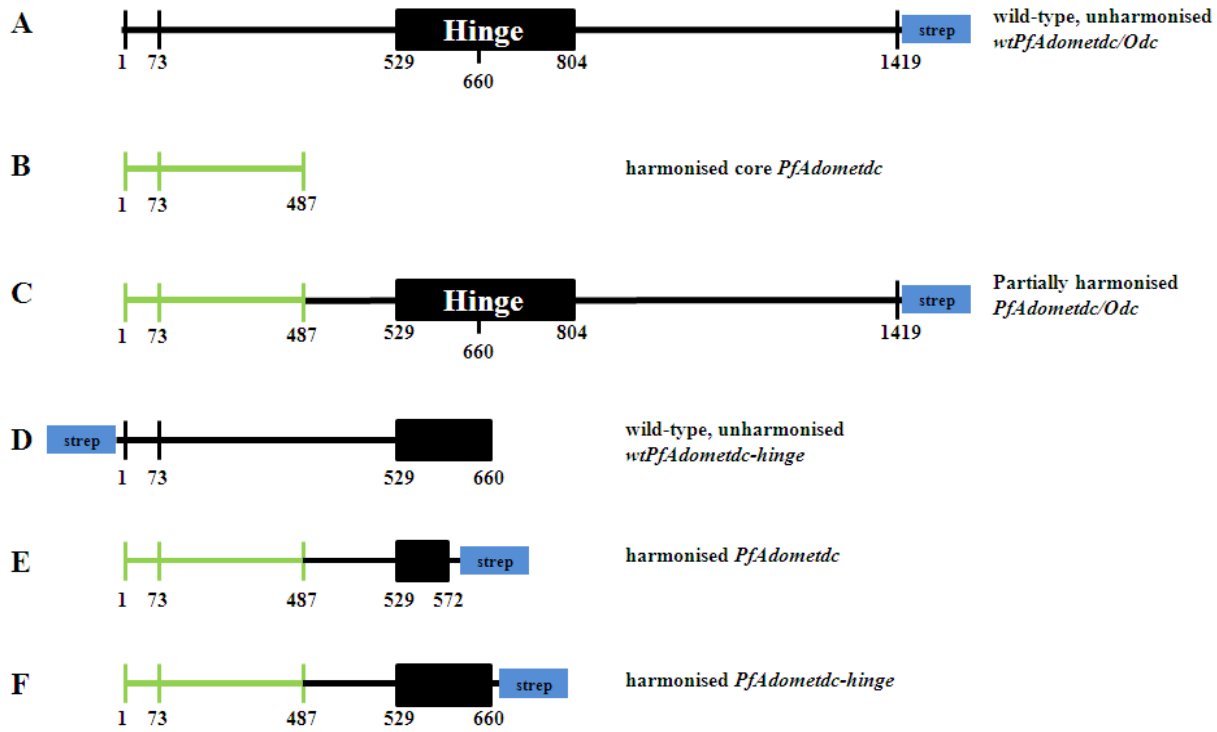

Figure 3.1: Schematic diagrams of the gene fragments used in the comparative *Pf*AdoMetDC protein expression study.
(A) The plasmid containing the wild-type, unharmonised full-length gene sequence (black line) of *PfAdometdc/Odc* [77] cloned into the pASK-IBA3 vector (C-terminal Strep-tag) was used to replace the core sequence of *PfAdometdc* with the codon-harmonised one (green line) in (B) to create a partially harmonised full-length gene (C). Two gene fragments were subsequently amplified from this partially harmonised full-length gene, namely (E) *PfAdometdc* (nucleotides 1-1716) encoding a C-terminally strep-tagged protein (572 residues) and (F) *PfAdometdc-hinge* (nucleotides 1-1980) encoding a C-terminally Strep-tagged protein (660 residues). The latter protein was compared to the expression of the (D) wt*Pf*AdoMetDC-hinge protein (660 residues) encoded from the wild-type, unharmonised gene (N-terminal Strep-tag) that was previously used in a study of the monofunctional *Pf*AdoMetDC protein [78].

The primers that were used for the amplification of these two fragments are listed in Table 3.1. PCR SuperMix (Invitrogen) was used with 5 fmol of template and 10 pmol of each of the forward and reverse primers. Temperature cycling was performed as follows: 94°C for 3 min, 85°C for 30 s followed by 25 cycles of 94°C for 30 s, 50°C for 1 min and 65°C for 4 min. The sizes of the PCR products were verified with DNA gel electrophoresis and the parental template DNA was removed by digestion with *Dpn*I (New England Biolabs) at 37°C for 1 h followed by digestion with *Bsa*I (New England Biolabs) at 50°C for 3 h. The pASK-IBA3 vector was also digested with *Bsa*I and used for the ligation with the *Bsa*I-digested PCR amplified fragments (pASK-IBA3 *PfAdometdc* and *PfAdometdc-hinge*). Ligation was carried out with T4 DNA Ligase at 4°C for 16 h. The ligated products were subsequently transformed into heat shock competent DH5α *E. coli* cells and positive colonies were selected using ampicillin resistance. Plasmids containing the harmonised *PfAdometdc* and *PfAdometdc-hinge* inserts were verified with automated nucleotide sequencing using a BigDye® Terminator v3.1 Cycle Sequencing kit (Applied Biosystems).

Table 3.1: Primers used for the amplification of the *PfAdometdc* and *PfAdometdc-hinge* fragments from the pASK-IBA3 containing partially harmonised *PfAdometdc/Odc*

Primer	Sequence (5' to 3')
domain_F	ATGGTAGGTCTCAAATGAATGGCATTTTCGAAGGCATTGAAA
domain_R	ATGGTAGGTCTCAGCGCTCAAAGTTTCTTTTTCTACACATTTAAC
hinge_R	ATGGTAGGTCTCAGCGCTATCTTTCTCATTTGTTTGTACCTTTTC

The expression constructs used for subsequent comparative protein expression therefore included the pASK-IBA7 vector containing wild-type, unharmonised *PfAdometdc* with half of the hinge region (Figure 3.1D, residues 1-660, N-terminal Strep-tag, wt*Pf*AdoMetDC-hinge) generously provided by Dr. C. Wrenger [71], the pASK-IBA3 vector containing harmonised *PfAdometdc* (Figure 3.1E, residues 1-572, C-terminal Strep-tag, *Pf*AdoMetDC) and the pASK-IBA3 vector containing harmonised *PfAdometdc* with half of the hinge region (Figure 3.1F, residues 1-660, C-terminal Strep-tag, *Pf*AdoMetDC-hinge).

3.2.2. Protein expression and purification

The plasmids containing unharmonised *wtPfAdometdc-hinge* [71], harmonised *PfAdometdc* and harmonised *PfAdometdc-hinge* were transformed into heat shock competent BL21 Star™ *E. coli* cells (Invitrogen). Colonies were inoculated in LB-ampicillin and incubated at 37°C for 16 h. These cultures were subsequently diluted 1:100 in 1 litre LB-ampicillin and incubated at 37°C with agitation. Protein expression was induced at an OD_{600} of 0.7-0.8 with 200 µg AHT (IBA). The cultures were incubated at 37°C for another 4 h before the cells were harvested. The pelleted cells were diluted in 10 ml wash buffer (100 mM Tris/HCl, pH 8.0, 150 mM NaCl, 1 mM EDTA) per litre of culture. Lysozyme and 0.1 mM PMSF was added to the suspension and incubated on ice for 30 min. The cells were subsequently disrupted with sonication and the soluble proteins were collected in the supernatants after ultracentrifugation was performed at 4°C for 1 h at 100 000*g*. The Strep-tagged fusion proteins (660-residue wt*Pf*AdoMetDC-hinge, 572-residue *Pf*AdoMetDC and 660-residue *Pf*AdoMetDC-hinge) were purified using Strep-*Tactin* affinity matrix (IBA) as described previously [69]. Samples of the insoluble proteins collected after ultracentrifugation were also kept for further analysis with SDS-PAGE and subsequent refolding from inclusion bodies (section 3.2.3).

The affinity-purified *Pf*AdoMetDC protein was separated with SEC using an Äkta Explorer System (Amersham Pharmacia Biotech). The Superdex®-S200 10/300 GL SE column (Tricorn, GE Healthcare) was calibrated with the Gel Filtration Standard kit (BioRad) that separated into five peaks corresponding to thyroglobulin (670 kDa), γ-globulin (158 kDa), ovalbumin (44 kDa),

myoglobin (17 kDa), and Vitamin B_{12} (1.35 kDa). The calibration curve was used to estimate protein sizes based on observed elution volumes (V_e). The column was subsequently equilibrated with filtered, degassed wash buffer after which protein samples (500 µl) were loaded and fractions corresponding to dimeric (~140 kDa) and monomeric (~70 kDa) *Pf*AdoMetDC were collected, pooled and subsequently concentrated with Amicon Ultra centrifugal filter devices (MWCO 3000, Millipore).

Protein concentrations were determined using protein absorbance at 280 nm and molar extinction coefficients of 69110 and 73580 M^{-1} cm^{-1} for *Pf*AdoMetDC and *Pf*AdoMetDC-hinge, respectively, followed by protein visualisation with SDS-PAGE using NuPAGE® 4-12% BisTris pre-cast gels (Invitrogen) and Colloidal Coomassie staining. Protein bands were identified with LC-MS/MS as previously described [8] as well as with Western immunodetection using monoclonal Strep-tag II mouse antiserum conjugated to HRP (Acris antibodies) (section 2.2.6).

3.2.3. Refolding of the *Pf*AdoMetDC from insoluble inclusion bodies

The cell pellets of the lysed cells from the expression of *Pf*AdoMetDC and *Pf*AdoMetDC-hinge were collected and analysed for the presence of the proteins in insoluble inclusion bodies [191]. The method of Sirawaraporn *et al*. was followed to isolate and refold the proteins from the insoluble fractions [192]. Briefly, the pellets were washed three times with wash buffer and the supernatants were discarded. The pellets were redissolved in wash buffer containing 20% (v/v) glycerol, 10 mM DTT, 0.2 M KCl and 6 M guanidinium hydrochloride. The tubes were rotated at 4°C for 1 h to unfold the proteins and subsequently refolded by adding drop-wise a 20-fold dilution of wash buffer containing 20% glycerol, 10 mM DTT and 0.2 M KCl. Refolding was performed overnight at 4°C with gentle stirring. The samples were then centrifuged and the supernatants were used in subsequent protein purification with Strep-*Tactin* affinity chromatography as previously described [69]. The protein eluates were visualised with SDS-PAGE and Colloidal Coomassie Staining.

3.2.4. Determination of enzyme activity and protein stability

The SEC-purified *Pf*AdoMetDC and wt*Pf*AdoMetDC-hinge enzymes were assayed for decarboxylase activity directly after purification and after two weeks of storage at 4 and -20°C. The assays were performed as previously described ([70] and section 2.2.4). Briefly, 5 µg (290 nM) protein was incubated in assay buffer (50 mM KH_2PO_4, pH 7.5, 1 mM EDTA, 1 mM DTT) and 100 µM substrate consisting of [*S*-(5'-adenosyl)-L-methionine chloride] (Sigma-Aldrich)

and 50 nCi AdoMet [*S*-(5'-adenosyl-[carboxy-^{14}C])-L-methionine] (55 mCi/mmol, Amersham Biosciences) in a total reaction volume of 250 µl. The reactions were incubated at 37°C for 30 min followed by reaction termination via protein precipitation with the addition of 30% (w/v) trichloroacetic acid. Specific enzyme activity was expressed as the amount of CO_2 produced in nmol/min/mg (or nmol/min per mol protein) and performed in duplicate for three individual experiments.

Differential scanning fluorimetry (DSF) was used to test a range of buffers (http://cassiopeia.maxlab.lu.se/index/dsf_screens/) that could contribute to the stability of the *Pf*AdoMetDC protein. Prior to protein stability screening of the SEC-purified *Pf*AdoMetDC protein, the wash buffer was exchanged with dialysis buffer (50 mM Tris/HCl, pH 8.0, 150 mM NaCl) to decrease the buffer strength and to remove the EDTA. A volume of 8.3 µl of each of the 24 buffers was pipetted into the ABgene® PCR plate (Thermo Scientific). The protein was diluted to a concentration of 0.15 mg/ml while the 100% DMSO-containing SYPRO orange dye (Sigma-Aldrich) was diluted 1:100 with H_2O. A volume of 25 µl protein containing 1:10 of the dye (final dilution of 1:1000) was added to each buffer-containing well, mixed briefly, and sealed with clear film. The plate was placed within the Mx3005P qPCR system (Stratagene) and the temperature was increased from 25°C to 95°C. Fluorescence readings with excitation and emission wavelengths of 492 nm and 610 nm, respectively, were measured at 1 min intervals [193]. The results were analysed with the MxPro software.

The stability of *Pf*AdoMetDC in the presence of the substrate analogues MDL73811 and CGP48664 was also tested. Protein (1.3 µM) was incubated with 1x, 5x, and 10x molar excesses of the two analogues for 30 min at RT. Volumes of 25 µl of the protein:ligand complexes as well as the protein without ligand were added in duplicate to the 96-well plate and analysed as before.

3.2.5. Investigations into the oligomeric status of monofunctional *Pf*AdoMetDC

3.2.5.1. Reducing and non-reducing SEC and SDS-PAGE

The oligomeric status of affinity-purified *Pf*AdoMetDC at concentrations of 1 mg/ml and 4 mg/ml were analysed with SEC as described in section 3.2.2. Monomeric and dimeric protein fractions collected from SEC were analysed in terms of their elution volumes (V_e) relative to the void volume (V_o) of the column (V_e/V_o). Reducing SEC was also performed by equilibrating the SE column with wash buffer containing 10 mM DTT. Monomeric (~70 kDa) and dimeric (~140 kDa) protein fractions collected from SEC were visualised with reducing (10 mM DTT added to

the sample buffer immediately prior to gel loading and electrophoresis) and non-reducing (reducing agent omitted from the sample buffer) SDS-PAGE.

3.2.5.2. MALDI-MS of affinity-purified proteins

Preliminary peptide mass fingerprinting with MALDI-MS was performed on the bands corresponding to the monomeric and dimeric proteins [191]. Protein sample extraction, dehydration and preparation for MALDI-MS as well as sample derivatisation with iodoacetamide to identify Cystines possibly involved in disulphide-bond formation, was performed as previously described [194]. Briefly, the gel bands were destained followed by dehydration with absolute ethanol and all samples except the dimeric ones were treated with 10 mM DTT in 50 mM NH_4HCO_3 for 30 min at 37°C. All samples were subsequently alkylated for 30 min with 55 mM iodoacetamide, washed with NH_4HCO_3 in 50% (v/v) ethanol and dehydrated as before. Trypsin digestion was performed overnight at 4℃ by using 96 ng trypsin in 50 mM NH_4HCO_3. The supernatants after the overnight digestion were collected and any remaining peptides were extracted with 50% ethanol and 50% (v/v) trifluoroacetic acid (TFA). The latter supernatants were pooled with the previously collected supernatants and dried *in vacuo*. The dried peptides were dissolved in 0.1% TFA and briefly centrifuged. A volume of 0.5 µl of each protein sample was directly spotted into the MALDI target plate, followed by the same volume of matrix solution (5 mg/ml α-cyano-4-hydroxycinnamic acid in 60% (v/v) acetonitrile and 0.1% TFA). MALDI-MS was performed using the Applied Biosystems 4700 Proteomics Analyzer with TOF/TOF™ optics in positive reflection mode. The peak lists were generated using T2D-exctractor with default settings and submitted to the MASCOT Peptide Mass fingerprint tool (http://www.matrixscience.com/).

3.2.5.3. Site-directed mutagenesis

Based on the MALDI-MS results the role of Cys505 in dimer stabilisation via covalent disulphide bond formation was studied by mutating the Cys codon to a Ser codon (M. Williams and [191]). The mutagenesis reaction to create the *PfAdometdc-C505S* mutant was performed by using the pASK-IBA3 plasmid containing harmonised *PfAdometdc* as template (Figure 3.1E) with the forward 5'-GGTAAAAGTTCCGTTTATTATCAAG-3' and reverse 5'-CTTGATAAT AAACGGAACTTTTACC-3' primers (mutations are underlined). Ex Taq™ DNA Polymerase (Takara Bio Inc.) was used to amplify the entire template [195] in the presence of 6 fmol template and 10 pmol of each of the primers. Temperature cycling was performed as follows: 95°C for 3 min followed by 25 cycles of 96°C for 30 s, 56°C for 30 s, 68°C for 5 min with a

final extension step at 68°C for 10 min. Post-PCR manipulation was performed as described previously [195]. Briefly, the PCR product was visualised with DNA gel electrophoresis and the correctly-sized band corresponding to the linear pASK-IBA3 plasmid containing *PfAdometdc* and the C505S mutation was purified with the Wizard® SV Gel and PCR Clean-up System (Promega). The agarose-purified product was then treated with *Dpn*I (Fermentas) for 3 h at 37°C and cleaned as before. The linear plasmids were directly electroporated into DH5α cells (Gibco BRL) and plated onto LB-ampicillin agar plates and incubated overnight at 37°C. Colonies were picked and grown for 16 h in LB-ampicillin (50 µg/ml) from which the plasmids were purified with the Zyppy™ Plasmid Miniprep kit (Zymoresearch). Positive clones were confirmed with restriction enzyme mapping and automated nucleotide sequencing using a BigDye® Terminator v3.1 Cycle Sequencing kit (Applied Biosystems).

3.2.5.4. Estimation of dimer dissociation constants

To estimate the order of magnitude of the dissociation constant (K_d) of the *Pf*AdoMetDC dimer (M. Williams and [191]) for comparison to other AdoMetDCs, the relative peak heights (and not areas due to peak overlaps) of the monomeric and dimeric proteins in the non-reducing SEC elution profiles (at concentrations of 1 mg/ml and 4 mg/ml of the wild-type and C505S mutant *Pf*AdoMetDC proteins) were assumed to approximately represent the relative proportions of monomer and dimer in the samples (X_M and X_D for monomer and dimer, respectively). Since the total amount of protein loaded was known the concentrations of the monomeric and dimeric proteins could be determined based on their relative proportions as analysed with SEC according to the following equations:

$$[M] = [C] \times X_M, [D] = \frac{M_0 - [M]}{2} = \frac{[C] \times X_D}{2}$$

Where M_0 is the total molar concentration, C is the protein concentration applied to the column in µM, and [M] and [D] are the molar concentrations in µM of the monomer and dimer, respectively.

Assuming simple monomer-dimer equilibrium (including Cys505 covalently-linked dimers) the dissociation constant of the dimeric protein could then be calculated by using the following formula:

$$K_a = \frac{[D]}{[M][M]} = \frac{1}{K_d}$$

Where K_d is the dissociation constant in units M and the association constant (K_a) in units M^{-1} is calculated by taking the inverse of K_d.

If the total protein concentration in a protein sample is known, the proportion of the monomeric form of the protein could subsequently be calculated as follows:

$$\frac{[M]}{M_0} = \frac{-1 \pm \sqrt{1+8(K_a)(M_0)}}{4(K_a)(M_0)}$$

Where $[M]/M_0$ is the proportion of the monomeric form of the protein and M_0 is the total molar concentration in units M.

3.2.5.5. Analyses of protein hydrodynamic radius with Dynamic Light Scattering

Dynamic light scattering (DLS) was used to determine the hydrodynamic radius of the *Pf*AdoMetDC and C505S mutant proteins as an indication of their oligomeric status. Fractions of the *Pf*AdoMetDC and C505S mutant proteins collected after SEC were pooled and concentrated to 2.8-6 mg/ml. Reduced *Pf*AdoMetDC was also analysed by treatment with 10 mM DTT prior to the DLS measurement. Additionally, DLS provides information on sample homogeneity as given by the polydispersity index (PdI). Immediately prior to measurements, the samples were centrifuged for 10 min at 10 000*g* to remove any aggregates. DLS was measured with the default settings of the Nanoziser Nano S instrument (Malvern Instruments). A 3 mm precision cell cuvette (Hellma) was used in which the protein samples with volumes of 15 µl were pre-equilibrated for 5 min at 20°C prior to the measurement. The theoretical R_H assuming globular protein shape were calculated with the Zetasizer Nano software v6.01 using default settings to determine the particle size distribution as given by the volume intensity plot.

3.2.6. Secondary structure analysis of *Pf*AdoMetDC using far-UV CD spectroscopy

The *Pf*AdoMetDC and C505S mutant proteins in wash buffer collected from SEC were dialyzed against a phosphate buffer (10 mM KH_2PO_4 pH 7.7, 50 mM NaF) for 3 h at 4°C due to the optical activity of Cl^- ions in the far-UV range [196]. Dialysis was performed using Slide-A-Lyzer® mini dialysis units (Thermo Scientific) each containing 150 µl of the protein sample. Following dialysis the concentrations of the samples were determined using protein absorbance at 280 nm and a molar extinction coefficient of 69110 M^{-1} cm^{-1}.

The far-UV spectra of the *Pf*AdoMetDC and C505S mutant proteins (0.5 mg/ml or 7.3 µM) were determined with the JASCO J815 CD instrument. Measurements were conducted in 1 mm cuvettes at a wavelength range of 190 to 250 nm at 20°C, using a wavelength interval of 0.5 nm, a bandwidth of 1 nm and a scanning speed of 20 nm/min. Two readings were accumulated per sample, buffer spectra were subtracted and the data points were averaged. The molar ellipticity ($[\theta]_M$) of each data point in units deg cm^2 $dmol^{-1}$ was calculated as follows according to Bale *et al*. [185]:

$$[\theta]_M = \frac{\Delta\theta \times MW}{10 \times l \times C}$$

Where $\Delta\theta$ is the reading in degree, MW is the molecular weight of the protein in g/mol, l is the path length in cm and C is the concentration of the protein in mg/ml.

The contribution of secondary structures were calculated with CDtool v1.4 [197].

3.2.7. Analyses of residues involved in the autocatalytic processing reaction

The alignment of the *PfAdometdc* gene sequence with the sequences from various organisms was previously performed by Wells *et al.* [120]. The corresponding residues involved in the processing of plant and human AdoMetDCs were identified and subsequently mutated on the gene sequence to determine if these play similar roles in the plasmodial protein. For all mutagenesis reactions partially harmonised *PfAdometdc/Odc* cloned into the pASK-IBA3 plasmid was used as template. The mutagenesis primers are listed in Table 3.2. Phusion DNA Polymerase (Finnzymes) was used in the presence of 6 fmol template and 10 pmol of each of the primers. Temperature cycling was performed as follows: 95°C for 3 min followed by 25 cycles of 96°C for 30 s, 56°C for 30 s, 68°C for 5 min with a final extension step at 68°C for 10 min. Post-PCR manipulation was performed as described previously [195].

Table 3.2: Primers used for the mutagenesis of residues predicted to be involved in the autocatalytic processing reaction of *Pf*AdoMetDC

Primer	Mutant name	Sequence (5' to 3') [a]
R11L_F	*Pf*AdoMetDC-R11L	GGCATTGAAAAACTCGTTGTC
R11L_R		GACAACGAGTTTTTCAATGCC
S421A_F	*Pf*AdoMetDC-S421A	CCATGCGGCTACGCCTGTAACG
S421A_R		CGTTACAGGCGTAGCCGCATGG

[a] Mutations are underlined.

3.2.8. *Pf*AdoMetDC enzyme and inhibition kinetics

The substrate affinity constant as well as V_{max} of the *Pf*AdoMetDC protein was determined using the Michaelis-Menten kinetic model. A substrate dilution series ranging from 12.5 to 800 µM were used to set up a Michaelis-Menten curve. Three independent experiments were performed in duplicate using the enzyme assay described above and the results were analysed with GraphPad Prism v5.0 (GraphPad Software, Inc.).

The linear Hanes-Woolf plot of substrate concentration ([S])/velocity (v) versus [S] was used to determine the K_m and V_{max} values [198]. The linear equation was obtained by a rearrangement of the Lineweaver-Burk equation:

$$\frac{[S]}{v} = \frac{[S]}{V_{max}} + \frac{K_m}{V_{max}}$$

Where the slope of the plot is equal to $1/V_{max}$, the intercept on the [S]/v axis gives K_m/V_{max} and the intercept on the [S] axis gives $-K_m$.

The inhibition kinetics of *Pf*AdoMetDC for two different substrate analogues, namely MDL73811 and CGP48664 were also repeated and compared with previous results of the monofunctional wt*Pf*AdoMetDC-hinge protein [71]. Based on literature studies and the mechanisms of inhibition of these two substrate analogues, irreversible and Michaelis-Menten kinetics were applied for MDL73811 and CGP48664, respectively [71].

The rate of enzyme inactivation by the irreversible MDL73811 inhibitor was followed by measurement of residual activity after fixed time intervals (0, 2, 4 and 6 min) of exposure to the inhibitor. *Pf*AdoMetDC enzyme (1 µg, 60 nM) was mixed with 0.1, 0.2 and 0.5 µM MDL73811 in the assay buffer at time point zero (25 µl), incubated at 37°C, stopped by transfer to ice and added to the reaction tubes containing 400 µM total AdoMet in a total volume of 225 µl. The reactions were subsequently incubated at 37°C for 30 min after which the experiment was carried out as before to determine the remaining enzyme activity after inhibition. The Kitz-Wilson method was used to determine the efficiency of the inhibitor [199]. The inhibition with time at the different inhibitor concentrations ([I]) were plotted against time as follows:

$$\ln\frac{E(t)}{E(0)} = \frac{-k_{inact} \times t}{1 + \frac{K_i}{[I]}} = -k_{app} \times t$$

Where E(t) is the maximal enzyme activity following pre-incubation with the inhibitor for time interval t; E(0) is the maximal enzyme activity following pre-incubation in the absence of inhibitor; and k_{app} is the slope obtained when the left hand side of the equation is plotted against time.

A secondary plot of the reciprocal of the k_{app} value (-1/primary slope) for each [I] against the reciprocal of [I] resulted in a straight line from which the k_{inact} and K_i values could be determined by the intercept and slope, respectively [198,200].

The inhibition of *Pf*AdoMetDC with CGP48664 was tested with the use of different substrate (100 to 800 µM) and inhibitor (2.5 to 10 µM) concentrations. These results were plotted on a typical Michaelis-Menten to obtain several hyperbolic curves for each [I] incubation at increasing [S]. The enzyme (1 µg, 60 nM) was incubated with 0, 2.5, 5 and 10 µM CGP48664 at each of the [S] for 30 min at 37°C to determine the remaining enzyme activity.

3.3. Results

3.3.1. Codon harmonisation improves the purity and stability of monofunctional *Pf*AdoMetDC

The 660-residue wt*Pf*AdoMetDC-hinge protein expressed from the unharmonised gene contains an N-terminal Strep-tag while the 572-residue *Pf*AdoMetDC protein expressed from the harmonised *PfAdometdc* gene contains a C-terminal Strep tag (Figure 3.1D and E). In this way the tag remains attached to the larger α-subunit after processing has occurred and is therefore not situated in proximate position of the active site co-factor (as is the case for the N-terminally tagged wild-type protein). Although not tested, the position of the Strep-tag may have an influence on enzyme activity but since the aim of this study was to obtain a high amount of pure, active protein a comparative study of the position of the tags were not considered.

Initially, only the first third of the bifunctional *PfAdometdc/Odc* gene was harmonised, which corresponds to the core of the monofunctional *Pf*AdoMetDC domain (Figure 3.1B, residues 1-487). Since the exact start site of the hinge region is unknown due to low sequence homology [120], an additional 255 nucleotides of the wild-type sequence (encoding residues 488-572) were added to obtain the harmonised *PfAdometdc* fragment (Figure 3.1E, *PfAdometdc* pASK-IBA3). In addition, to allow for a comparative analysis of the monofunctional construct created here and a previous study on the monofunctional protein (Figure 3.1D, wt*Pf*AdoMetDC-hinge, residues 1-660) [71], a second expression construct was created to encode a 660-residue *Pf*AdoMetDC-hinge protein where residues 1-487 are encoded by the harmonised codons (Figure 3.1F, *PfAdometdc-hinge* pASK-IBA3).

The *Pf*AdoMetDC, *Pf*AdoMetDC-hinge and wt*Pf*AdoMetDC-hinge proteins were expressed in BL21 Star™ *E. coli*. Figure 3.2 shows the results obtained when the expression of these three proteins were compared. In each case, two subunits are expected to separate with the denaturing conditions of SDS-PAGE as a result of *Pf*AdoMetDC autocatalytic processing. These include the smaller ~9 kDa β-subunit (not resolved with the 7.5% acrylamide gel) and the larger α-subunit. The different lengths of the expressed proteins will be reflected by the sizes of the α-subunits; for the 572-residue *Pf*AdoMetDC protein (Figure 3.2, top right) this subunit is predicted to have a size of ~61 kDa while the *Pf*AdoMetDC-hinge proteins (expressed from wild-type, top left, and harmonised genes, bottom right) would have α-subunits that are ~10 kDa larger. For the latter two proteins a difference would additionally be the positions of the Strep-tags as shown in the diagrams (Figure 3.2, inset figures).

Expression of the wt*Pf*AdoMetDC-hinge protein resulted in the presence of the ~70 kDa processed protein (Figure 3.2A, lane 1, band b) where the β-subunit at the N-terminus (containing the Strep-tag) dissociates from the larger α-subunit and was therefore not resolved with the applied denaturing PAGE conditions. However, wt*Pf*AdoMetDC-hinge co-purified with an approximately equal amount of *E. coli* heat shock protein 70 (Hsp70) as identified with LC-MS/MS (Figure 3.2A, lane 1, band a), even after extensive optimisation of various conditions during protein expression and purification. Malarial proteins expressed in *E. coli* are often co-purified with HSPs, which gives an indication of the stress that is placed on the system during folding of these proteins [190].

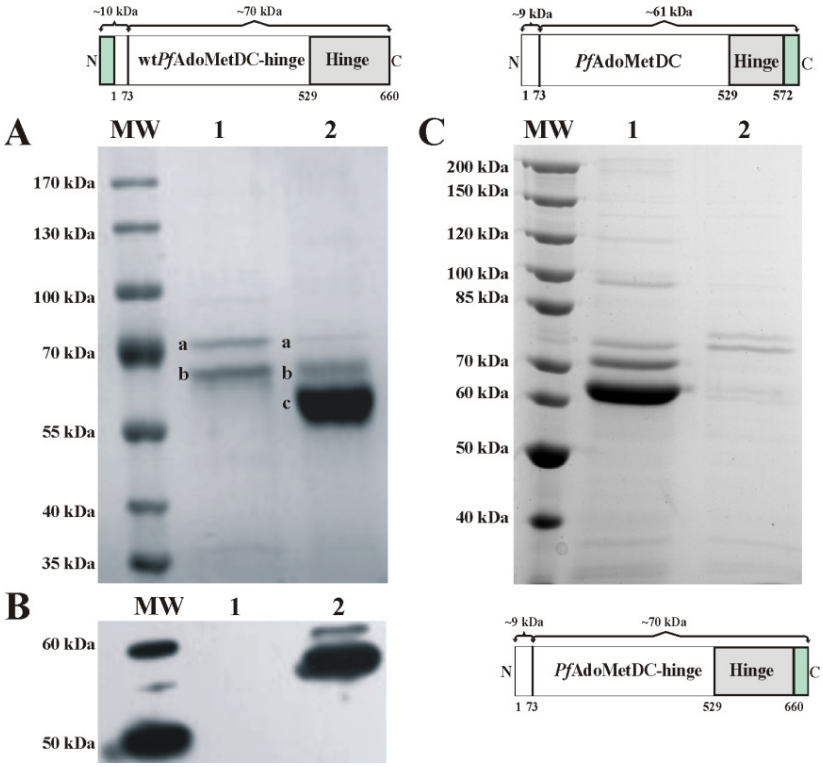

Figure 3.2: SDS-PAGE analyses of *Pf*AdoMetDC, *Pf*AdoMetDC-hinge and wt*Pf*AdoMetDC-hinge proteins followed by Western immunodetection of these recombinantly expressed monofunctional proteins.
(A) SDS-PAGE analysis of wt*Pf*AdoMetDC-hinge and *Pf*AdoMetDC proteins. MW: PageRuler Prestained Protein Ladder; lane 1: wt*Pf*AdoMetDC-hinge protein expressed from the wild-type, unharmonised gene; band a: Hsp70; band b: α-subunit of wt*Pf*AdoMetDC-hinge. Lane 2: *Pf*AdoMetDC protein expressed from the harmonised gene; band a: Hsp70; band b: unprocessed *Pf*AdoMetDC protomer; band c: α-subunit of *Pf*AdoMetDC. (B) Western immunodetection of wt*Pf*AdoMetDC-hinge (lane 1) and *Pf*AdoMetDC (lane 2) proteins with a Strep-tag antibody. (C) SDS-PAGE analyses of the *Pf*AdoMetDC (lane 1) and *Pf*AdoMetDC-hinge (lane 2) proteins expressed form harmonised genes. The schematic diagrams of the three proteins are also included to show the predicted sizes of the α- and β-subunits of each as well as the positions of the Strep-tags (light green boxes).

*Pf*AdoMetDC separates as a ~61 kDa α-subunit and a ~9 kDa β-subunit and resulted in an almost 10-fold improvement in yield (39.6 µg/ml versus 385.1 µg/ml) of the affinity-purified protein compared to total protein yield obtained for the wt*Pf*AdoMetDC-hinge protein. Of this,

particularly the ~61 kDa processed form of the protein was present, proven by LC-MS/MS analyses to consist of only *Pf*AdoMetDC (Figure 3.2A, lane 2, band c). This protein expressed from the harmonised construct is therefore in a more pure form at a higher yield. However, the results showed that a fraction of the *Pf*AdoMetDC protein was present in its unprocessed ~70 kDa protomeric form (Figure 3.2A, lane 2, band b). A decrease in co-purification of contaminating Hsp70 was also observed (Figure 3.2A, lane 2, band a).

Western immunodetection using a Strep-tag antibody confirmed the presence of the *Pf*AdoMetDC protein (Figure 3.2B, lane 2), while no protein was identified for wt*Pf*AdoMetDC-hinge due to the cleaved ~10 kDa β-subunit with the N-terminal Strep-tag, which was not resolved on this gel (Figure 3.2B, lane 1).

In comparison to *Pf*AdoMetDC, expression of the *Pf*AdoMetDC-hinge protein yielded much less protein (40.3 µg/ml), which is similar to the yield obtained for the wt*Pf*AdoMetDC-hinge protein. SDS-PAGE analysis showed the presence of two major bands that, in the absence of LC-MS/MS analyses, could represent the processed (~70 kDa) and unprocessed (~79 kDa) forms of the protein and/or Hsp70 (Figure 3.2C, lane 2).

3.3.2. Refolding of *Pf*AdoMetDC from inclusion bodies yields a significant amount of unprocessed protein

Protein purification from the soluble extracts of the proteins expressed from codon-harmonised genes (*PfAdometdc* and *PfAdometdc-hinge*) indicated that in the heterologous expression system the processing reaction was not 100% efficient since the unprocessed form of the *Pf*AdoMetDC protein was retrieved (Figure 3.2A, lane 2, band b). Subsequent SDS-PAGE analyses of the proteins obtained from the insoluble protein extract showed that an appreciable amount of *Pf*AdoMetDC is expressed as insoluble protein (Figure 3.3A) while, in comparison to the protein preparation from the soluble extract (Figure 3.2C), most of *Pf*AdoMetDC-hinge was expressed as insoluble protein in inclusion bodies (Figure 3.3B).

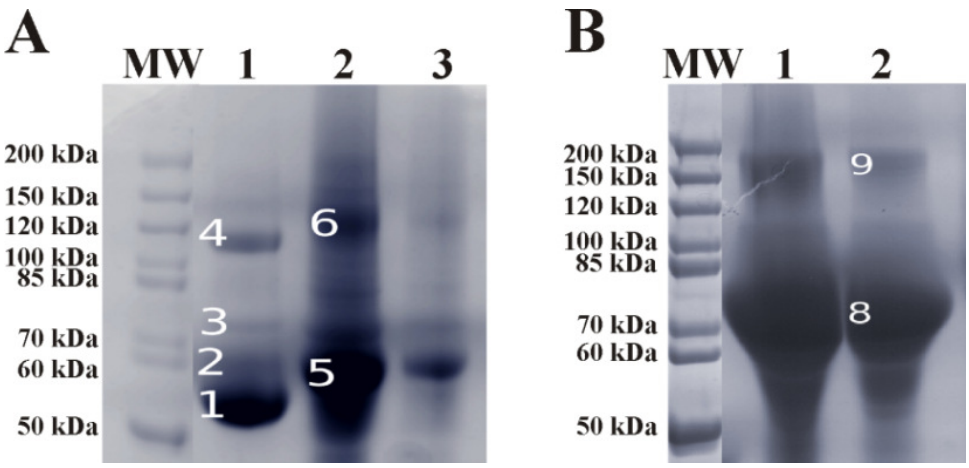

Figure 3.3: Non-reducing SDS-PAGE analyses of the insoluble protein extracts of expressed (A) *Pf*AdoMetDC and (B) *Pf*AdoMetDC-hinge proteins.
The insoluble protein extracts of (A) *Pf*AdoMetDC and (B) *Pf*AdoMetDC-hinge were collected after ultracentrifugation of the lysed expression cells. The numbers indicate the proteins that were identified with MALDI-MS (section 3.3.4.1). MW: PageRuler Unstained Protein Ladder. Gel (A) lane 1: *Pf*AdoMetDC isolated from the soluble protein extract with Strep-tag affinity chromatography; lane 2: sample from the insoluble protein pellet after expression of *Pf*AdoMetDC; lane 3: 10-fold dilution of the insoluble protein pellet in lane 2. Gel (B) lane 1: sample from the insoluble protein pellet after expression of *Pf*AdoMetDC-hinge and lane 2: 10-fold dilution of the insoluble protein pellet in lane 1.

The refolding and purification of the monofunctional *Pf*AdoMetDC and *Pf*AdoMetDC-hinge proteins within the insoluble inclusion bodies were subsequently performed by applying the method of Sirawaraporn *et al*. [192] to determine if correct refolding under favourable *in vitro* conditions could lead to efficient processing of *Pf*AdoMetDC into the active form of the protein. Concurrently, proteins were also isolated from the soluble protein extracts for comparison. The yields that were obtained per litre of protein culture for each protein preparation are listed in Table 3.3.

Table 3.3: Yields obtained for the *Pf*AdoMetDC and *Pf*AdoMetDC-hinge proteins isolated from soluble and insoluble protein extracts

Protein preparation	Concentration (mg/ml)	Yield (mg)
*Pf*AdoMetDC soluble	0.71	4.26
*Pf*AdoMetDC insoluble	0.28	1.68
*Pf*AdoMetDC-hinge soluble	0.22	1.32
*Pf*AdoMetDC-hinge insoluble	0.37	2.22

The highest yield obtained was for the *Pf*AdoMetDC protein isolated from the soluble protein extract but another 1.68 mg could be recovered from the insoluble extract (Table 3.3). For *Pf*AdoMetDC-hinge more protein could be isolated from the insoluble protein extract, which represented a promising result since a low protein yield was isolated from the soluble fraction presumably due to the presence of the hinge region (Figure 3.2C).

SDS-PAGE analyses showed that the purification of the *Pf*AdoMetDC and *Pf*AdoMetDC-hinge proteins from the inclusion bodies resulted in the successful retrieval of protein. For *Pf*AdoMetDC a single protein band with a size of ~70 kDa was observed (Figure 3.4A, lane 5) while a band at ~79 kDa was observed for the *Pf*AdoMetDC-hinge sample (Figure 3.4A, lane 6). The sizes of these bands indicated the presence of only the unprocessed protomers in both samples. In the absence of Hsp70, other contaminating proteins were co-purified, which could probably be removed with secondary purification steps. In order to ascertain that only the unprocessed proteins were purified, SDS-PAGE with a higher acrylamide % gel was also performed. These results showed that, compared to the soluble expression of *Pf*AdoMetDC (Figure 3.4B, lane 1), the ~9 kDa subunits were absent in both protein samples obtained from the inclusion bodies (Figure 3.4B, lanes 2 and 4) and indicates that the conformation of the proteins were not correct to allow processing to occur via the Arg11-Lys15-Lys215 triad [120].

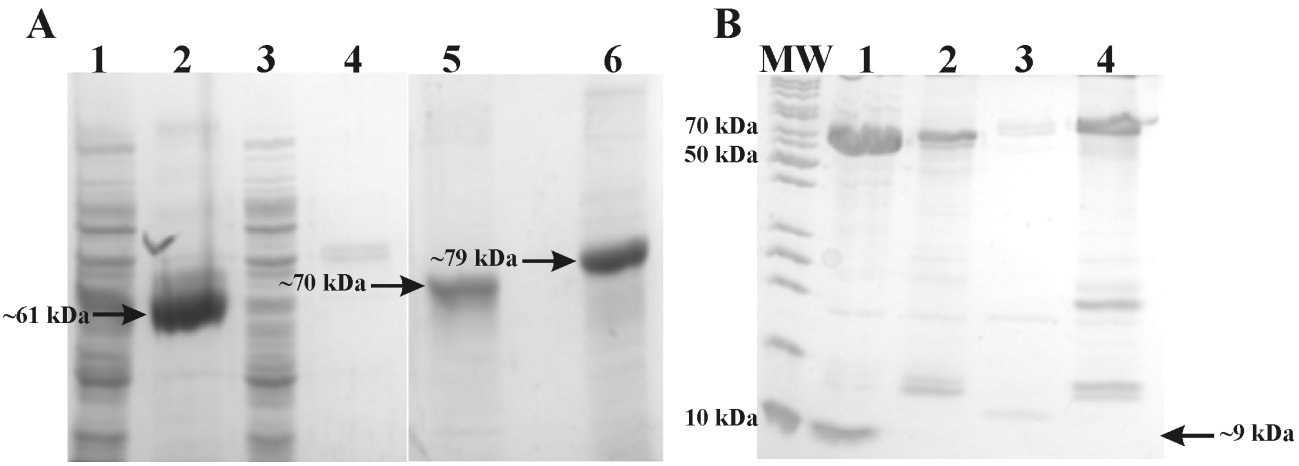

Figure 3.4: Purification of *Pf*AdoMetDC and *Pf*AdoMetDC-hinge from inclusion bodies and visualisation on 7.5% (A) and 12.5% (B) SDS-PAGE gels.
Gel (A) lane 1: *Pf*AdoMetDC total soluble; lane 2: Strep-tag purified *Pf*AdoMetDC from soluble extract; lane 3: *Pf*AdoMetDC-hinge total soluble; lane 4: Strep-tag purified *Pf*AdoMetDC-hinge from soluble extract; lane 5: Strep-tag purified *Pf*AdoMetDC refolded from insoluble extract; lane 6: Strep-tag purified *Pf*AdoMetDC-hinge refolded from insoluble extract. Gel (B) MW: PageRuler Unstained Protein Ladder; lane 1: Strep-tag purified *Pf*AdoMetDC from soluble extract; lane 2: Strep-tag purified *Pf*AdoMetDC refolded from insoluble extract; lane 3: Strep-tag purified *Pf*AdoMetDC-hinge from soluble extract; lane 4: Strep-tag purified *Pf*AdoMetDC-hinge refolded from insoluble extract. The sizes of the protein bands are indicated with arrows.

3.3.3. *Pf*AdoMetDC enzyme activity and protein stability

Due to these disappointing results obtained for the *Pf*AdoMetDC-hinge protein isolated from the soluble extract, subsequent experiments were performed on *Pf*AdoMetDC for its comparison to the expression of the wt*Pf*AdoMetDC-hinge protein.

*Pf*AdoMetDC has a specific activity of 140±8 nmol/min per nmol protein compared to wt*Pf*AdoMetDC-hinge with an activity of 88±4 nmol/min/nmol (of which approximately half of

the protein sample is Hsp70, Figure 3.2A). Furthermore, *Pf*AdoMetDC appeared to be a more stable enzyme than wt*Pf*AdoMetDC-hinge since this enzyme remained active when stored for two weeks at 4 and -20°C. In contrast, wt*Pf*AdoMetDC-hinge activity was significantly reduced by 16% and 55% (n=2, $P<0.05$) at 4 and -20°C, respectively (Table 3.4).

Table 3.4: Comparison of the *Pf*AdoMetDC and wt*Pf*AdoMetDC-hinge enzyme activities after storage for two weeks at different temperatures
Mean specific activities in nmol/min/per nmol protein were determined from two independent experiments carried out in duplicate (n=2) and are shown with ± S.E.M.

Enzyme	Day 1	Day 14 (4°C)	Day 14 (-20°C)
***Pf*AdoMetDC**	140±8	165.8±2.8	184±9
wt*Pf*AdoMetDC-hinge	88±4	74±10	39.7±1.5

DSF was subsequently performed to determine if the stability of the *Pf*AdoMetDC protein could be improved with a specific buffer system for efficient protein storage. The DSF results showed a general decrease in the Tm of *Pf*AdoMetDC with an increase in buffer pH. Buffers containing MES, ammonium acetate or BisTris propane at a pH ~6.0 promoted protein stability to the same extent, and the addition of glycerol did not result in improved protein stabilisation (results not shown). These results were subsequently compared to the dialysis buffer (50 mM Tris/HCl, pH 8.0, 150 mM NaCl) to determine if a difference in protein stability exists with this buffer compared to the most promising buffer identified with DSF (0.4 M MES, pH 6.0, 0.6 M NaCl). The results showed that the Tm of the protein in a buffer where the pH was increased from 6.0 to 8.0 or where Tris/HCl in the dialysis buffer was exchanged with BisTris propane remained similar (62°C versus 61°C) and a different buffer system was therefore not considered for future experiments in which a stable protein is required.

The subsequent co-incubation of *Pf*AdoMetDC with two substrate analogues, MDL73811 or CGP48664, showed that molar excesses of either analogue increased the Tm from 62°C to 66°C compared to the apo-protein with a Tm of 62°C (Figure 3.5). These results indicated improved protein stability for the ligand-bound form of the protein.

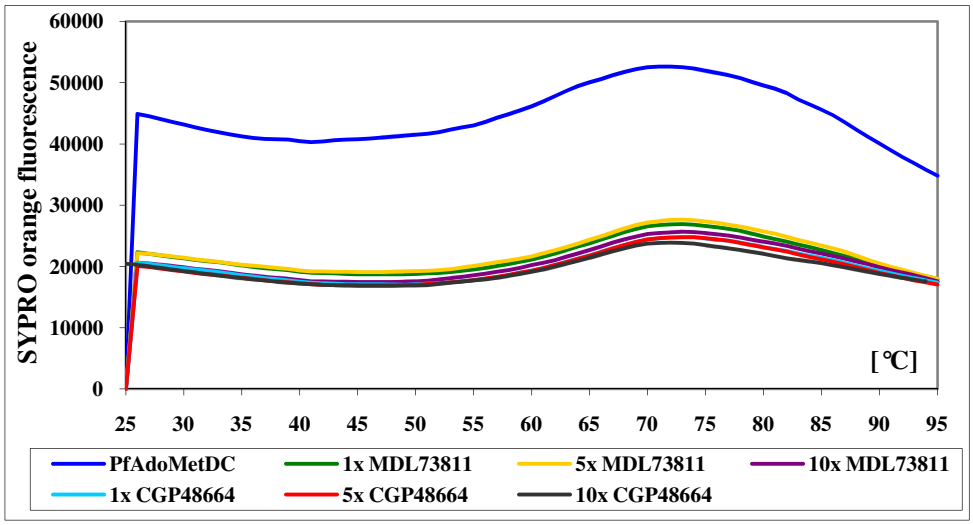

Figure 3.5: Fluorescence intensity curves obtained upon incubation of *Pf*AdoMetDC with different molar excesses of MDL73811 and CGP48664.
Incubation of *Pf*AdoMetDC (1.3 µM) in dialysis buffer with MDL73811 and CGP48664 at three different molar excesses (1x, 5x and 10x) of the substrate analogues were tested to determine their effect on the protein's stability as recorded by the Tm. Fluorescence intensities of the SYPRO orange dye bound to the hydrophobic surfaces of the protein were obtained while the temperature was increased from 25°C to 95°C [193].

3.3.4. Determination of the oligomeric status of monofunctional *Pf*AdoMetDC

Purification of the *Pf*AdoMetDC protein with affinity chromatography allowed further analyses with SEC to determine its oligomeric status. A Superdex S200 column was calibrated from which a calibration curve with a regression coefficient of R^2=0.98 could be obtained. Strep-tag purified *Pf*AdoMetDC protein separated by SEC is expected to elute at a V_e of the dimeric protein (~140 kDa) in the elution fraction range 12-13 ml (V_e/V_o of ~1.5-1.625) while the monomer (~70 kDa) is expected to elute between 14 and 15 ml (V_e/V_o of ~1.75-1.875).

Concentration-dependent monomer-dimer equilibrium is evident for *Pf*AdoMetDC since at 1 mg/ml both monomeric (V_e/V_o of 1.77, calculated MW of ~85 kDa) and dimeric (V_e/V_o of 1.59, calculated MW of ~120 kDa) forms of the protein are present (Figure 3.6A, solid line). At a 4-fold higher concentration of the protein and in the absence of DTT, the proportion of the dimeric fraction (V_e/V_o of 1.60, ~114 kDa) increases relative to that of the monomer (V_e/V_o of 1.73, ~87 kDa). (Figure 3.6A, dotted line). Apart from the peak representing aggregated protein at the void volume (8 ml), a larger oligomer also forms at the shoulder of the dimeric protein peaks (V_e/V_o of 1.44, ~180 kDa) at both protein concentrations tested and could represent a trimeric form of the protein.

Dimerisation as a result of the oxidising conditions was subsequently analysed with the addition of 10 mM DTT to the protein (3-5 mg/ml) prior to SEC, which resulted in a significant shift from

a dimer at an V_e of 12.8 ml (V_e/V_o of 1.61, ~131 kDa) to the monomeric form with an V_e of 13.4 ml (V_e/V_o of 1.68, ~99 kDa) (Figure 3.6B, solid line). A protein sample collected from the dimeric protein peak and visualised with non-reducing SDS-PAGE showed that the intensity of the dimeric protein band was vastly reduced when 10 mM DTT was added to the sample buffer and confirmed the shift of the dimer to the monomeric form under reducing conditions (Figure 3.6C). These results showed that increasing the concentration of the *Pf*AdoMetDC protein increased the proportion of the dimeric protein relative to that of the monomer while higher oligomeric forms are also formed. However, both the SDS-PAGE and SEC results show a slight increase in the apparent molecular weight of the reduced protein compared to the non-reduced monomeric protein, which was also confirmed by DLS (see below). The increased proportion of dimeric *Pf*AdoMetDC under non-reducing conditions suggests the involvement of Cys residue/s on the protein surface in disulphide bond/s formation between the *Pf*AdoMetDC monomers, which is enhanced when the protein is present at concentrations >1 mg/ml.

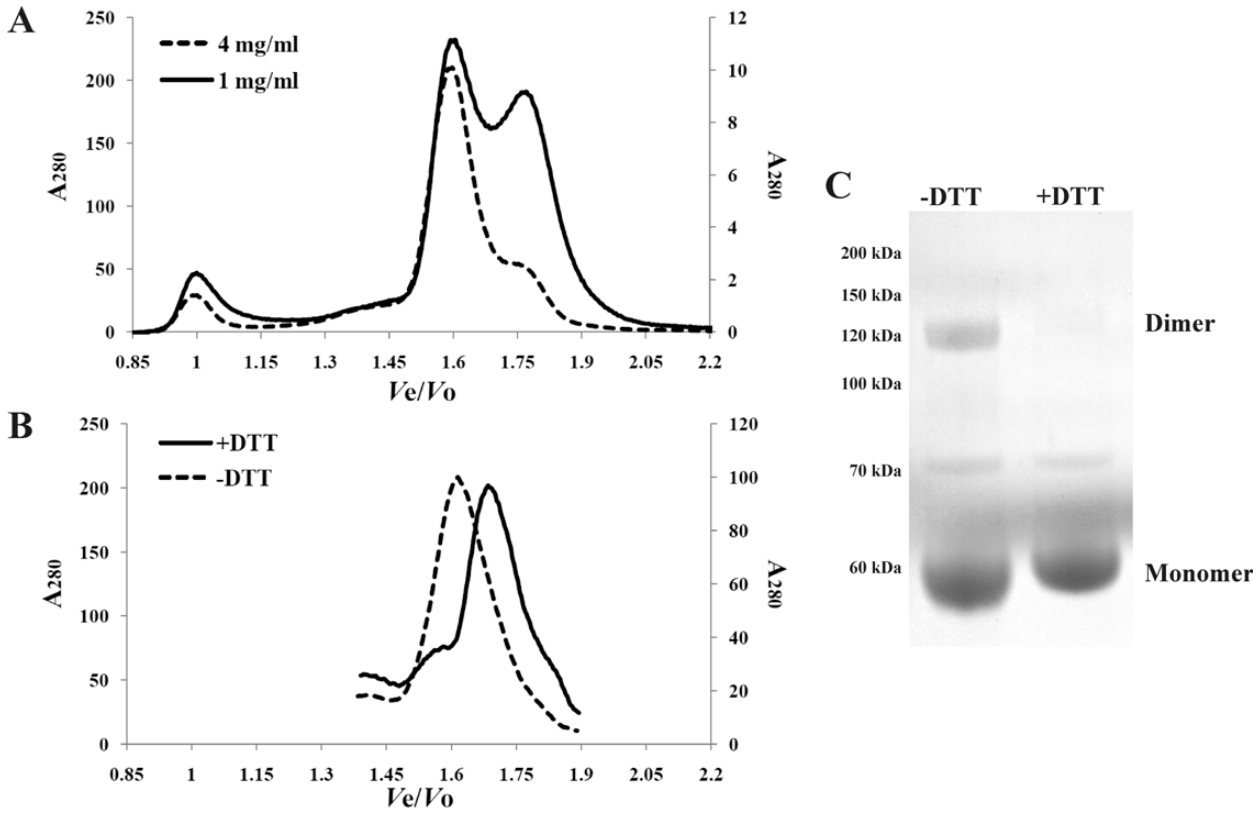

Figure 3.6: Analyses of the oligomeric status of monofunctional *Pf*AdoMetDC with SEC.
(A) The *Pf*AdoMetDC protein purified with Strep-tag affinity chromatography at concentrations of 1 mg/ml and 4 mg/ml were separated with SEC. The fractions corresponding to the dimeric and monomeric proteins are indicated. The V_e/V_o values are shown on the X-axis while the Y-axes on the left and right of the graph shows the absorbance at 280 nm for the higher or lower concentrated protein samples, respectively. (B) Reducing SEC was performed in the presence or absence of 10 mM DTT, followed by visualisation with non-reducing SDS-PAGE of the 4 mg/ml protein sample in the presence or absence of 10 mM DTT (C). The sizes of the protein ladder as well as the positions of the dimeric and monomeric proteins are shown. Lane 1: no DTT and lane 2: 10 mM DTT included in sample buffer.

Stabilisation of the monomeric form of the protein under reducing conditions was confirmed with DLS analyses. Treatment of *Pf*AdoMetDC with DTT reduced the R_H and therefore the size of the protein. The protein sample showed radii of 7.33 nm and 9.07 nm in the presence and absence of DTT, respectively (Table 3.5). This corresponds to a decrease of ~20% in both *Pf*AdoMetDC protein diameter and PdI, indicating a fairly monodisperse protein sample since DTT causes a shift in the equilibrium from the dimer to the monomer.

Table 3.5: Hydrodynamic radii of *Pf*AdoMetDC in the presence and absence of DTT as determined by DLS
*Pf*AdoMetDC samples at a concentration of 2.8 mg/ml with and without DTT were analysed by DLS and the level of polydispersity was indicated by the PdI value.

Protein sample	Concentration (mg/ml)	R_H (nm)	PdI
*Pf*AdoMetDC -DTT	2.8	9.07	0.23
*Pf*AdoMetDC +DTT	2.8	7.33	0.18

These results suggest that disulphide linkage either induces changes in protein conformation, which is not readily reversed by DTT treatment alone or reflects the average radius of a mixture of the monomeric and dimeric forms of the protein. Alternatively, the increase in protein apparent size could be due to DTT binding to the protein [201,202] although the likelihood that reduction of inner disulphide bonds by DTT that could affect a shape change from e.g. globular to a more expanded and thus a larger size protein [203], cannot be excluded.

3.3.4.1. Cys505 stabilises *Pf*AdoMetDC dimerisation

Inspection of the proposed dimer interface of the *Pf*AdoMetDC homology model [120] showed the possible involvement of Cys505 from each monomer in disulphide bond formation. This residue is not conserved amongst the AdoMetDCs but structure-based sequence alignment indicated that residue Cys505, which is located on the β15 strand at the proposed dimer interface of *Pf*AdoMetDC, could form a disulphide bond with the same residue from a second monomer. Cys505 in *P. falciparum* AdoMetDC corresponds to Gln311 in the human protein. Gln311 is also located on the β15 strand at the dimer interface of the human protein with a distance of 6.68 Å between the C_δ atoms and, considering the distance between the residues, could theoretically also form a disulphide bond if replaced by Cys residues as in *Pf*AdoMetDC.

To ascertain if Cys505 mediated disulphide bond formation resulting in the appearance of dimeric proteins under oxidising conditions, MALDI-MS peptide mass fingerprinting was performed on the ~120 kDa SDS-resistant dimeric band (Figure 3.7, lane C, band 7), which was

treated with iodoacetamide prior to trypsin digestion both in the presence and in the absence of DTT. Exposed Cys residues would thereby be modified by alkylation while residues involved in disulphide bonds (and not treated with DTT) should be protected resulting in corresponding peptide mass differences. As a control for non-disulphide linked proteins, the monomeric ~61 kDa band was also analysed (Figure 3.7, Lane C, band 4). The MALDI-MS peptide mass fingerprints of the ~120 kDa dimeric band in Figure 3.7 without reduction prior to alkylation was compared to the fingerprints of the dimeric and monomeric bands that were reduced and alkylated after purification from SDS-PAGE.

The results confirmed that the carbamidomethyl-modified Cys505 residue could only be identified in the reduced, alkylated condition and in the mass spectrum of the monomeric band (Figure 3.7). Furthermore, no peptide fragments containing alkylated Cys47, 143, 418, 454 and 481 were identified as these are, like Cys505, surface-localised based on the *Pf*AdoMetDC homology model (results not shown) [120].

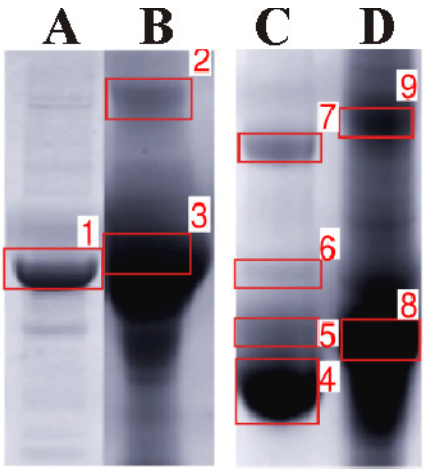

Protein band	DTT	Cys505 fragment	MASCOT search	MASCOT score
1	Y	-	gi|67462335|	337
2	N	ND	gi|124802819|	117
3	Y	ND	gi|124802819|	149
4	Y	ND	gi|124802819|	123
5	Y	1417.67 Da	gi|124802819|	119
6	Y	-	gi|67462335|	319
7	N	ND	gi|124802819|	133
	Y	1417.62 Da	gi|124802819|	145
8	Y	ND	gi|124802819|	109
9	N	ND	gi|124802819|	124
	Y	1417.62 Da	gi|124802819|	192

Figure 3.7: Protein gel bands of the *Pf*AdoMetDC and *Pf*AdoMetDC-hinge proteins that were analysed with MALDI-MS.
Proteins that were eluted for trypsin digestion were extracted from two gels. Lane A: *Pf*AdoMetDC-hinge purified with Strep-tag affinity chromatography (band 1); Lane B: the insoluble protein extract after *Pf*AdoMetDC-hinge expression (bands 2 and 3); Lane C: *Pf*AdoMetDC purified with Strep-tag affinity chromatography (bands 4-7); and Lane D: the insoluble protein extract after *Pf*AdoMetDC expression (bands 8 and 9). The protein bands are numbered and the results of the MALDI-MS analyses are shown in the table corresponding to each protein band. The addition of 10 mM DTT during protein preparation for analyses is indicated in the table as yes (Y) or no (N). The detection of a protein fragment containing Cys505 as an indication of a non-disulphide linked protein is indicated in the table as (-) not applicable for the Hsp70 protein, (ND) for not detected i.e. Cys505 could be involved in disulphide bond formation and if Cys505 was detected the size of the fragment in which it was identified is given i.e. as an indication that Cys505 could be in its reduced form in the presence of DTT. The gene accession numbers of the MASCOT search together with the MASCOT scores of the peptides are given as gi\|67462335\| for *Hsp70 E. coli* and gi\|124802819\| for *Adometdc/Odc P. falciparum*.

To further elucidate the possible involvement of Cys505 in disulphide bond formation, a mutant

protein was created in which this residue was changed to a Ser. While the expression level (Figure 3.8A) and specific activity of *Pf*AdoMetDC-C505S was identical compared to the wild-type *Pf*AdoMetDC (results not shown), the addition of DTT once again resulted in a larger apparent size of the protein (Figure 3.8A) compared to the non-reduced samples (Figure 3.8B) of both the wild-type and mutated monomeric proteins. Subsequent SEC of the mutant protein at a concentration of 1 mg/ml and under non-reducing conditions showed that the *Pf*AdoMetDC-C505S protein occurs mainly in its monomeric form (V_e/V_o of 1.74) (Figure 3.8C, solid line). However, the equilibrium was again shifted towards dimer formation at a concentration of 4 mg/ml (V_e/V_o of 1.64) (Figure 3.8C, dotted line). These results indicate that the *Pf*AdoMetDC protein is still able to dimerise even in the absence of covalently-linked dimers.

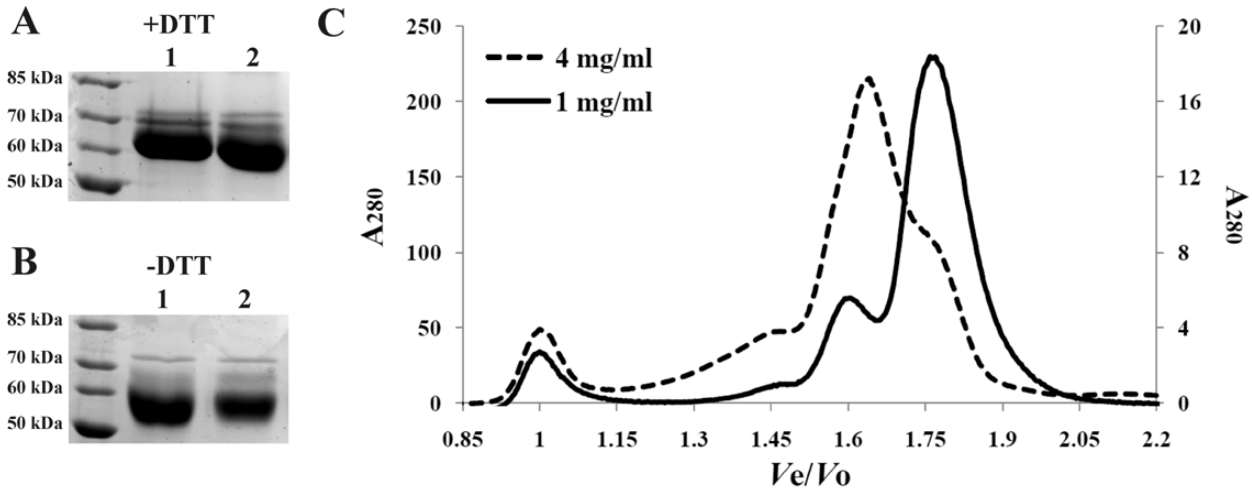

Figure 3.8: Analyses of the oligomeric status of the C505S mutant of *Pf*AdoMetDC with SEC.
(A) Reducing and (B) non-reducing SDS-PAGE of the *Pf*AdoMetDC (lane 1) and C505S mutant (lane 2) proteins. The sizes of the protein ladder are shown. (C) Analyses of the oligomeric status of the *Pf*AdoMetDC-C505S mutant protein purified with Strep-*Tactin* affinity chromatography and at concentrations of 1 and 4 mg/ml with SEC. The V_e/V_o values are shown on the X-axis while the Y-axes on the left and right of the graphs show the absorbance at 280 nm for the higher and lower concentrated protein samples, respectively.

To gain further insight into the affect of the Cys505 mutation on protein dimerisation, DLS was performed to determine the particle size of the mutant protein. DLS showed a radius of 5.79 nm for the C505S mutant in the absence of DTT (3 mg/ml), while treatment of *Pf*AdoMetDC at a concentration of 2.8 mg/ml with DTT only decreased the hydrodynamic radius from 9.07 to 7.33 nm (Table 3.5). The mutant protein therefore has a diameter 36% less than that of the wild-type protein, which indicates a smaller particle size of the mutant (Table 3.6). The results show that DTT treatment alone was not as effective as the C505S mutation in stabilising the monomeric form of the protein and therefore reflects an average radius of a mixture of the monomeric and dimeric forms of the wild-type protein resulting in a hydrodynamic radius of 7.33 nm.

Table 3.6: Hydrodynamic radii of *Pf*AdoMetDC-C505S at two different protein concentrations

Protein sample	Concentration (mg/ml)	R_H (nm)	PdI
*Pf*AdoMetDC-C505S	3	5.79	0.12
*Pf*AdoMetDC-C505S	6.8	6.96	0.13

The more dilute *Pf*AdoMetDC-C505S protein showed the smallest diameter as well as the lowest PdI (Tables 3.5 and 3.6) and increasing the protein concentration to 6.8 mg/ml only resulted in a slight increase in the PdI, which was still below that of the wild-type *Pf*AdoMetDC protein (Table 3.5) and indicates good sample monodispersity.

3.3.4.2. Estimated dissociation constants of *Pf*AdoMetDC and the C505S mutant

SEC results showed the presence of both monomeric and dimeric forms of the *Pf*AdoMetDC and C505S mutant proteins. The peaks were not clearly separated but the peak maxima could be clearly identified. In the absence of analytical tools, the SEC results (Figures 3.6 and 3.8) were used to estimate a range of the dissociation constants for the two proteins while keeping in mind that equal amounts of the monomers and dimers were not present. Additionally, simple monomer-dimer equilibrium was assumed where, in the absence of DTT, residues Cys505 could form covalently-linked dimers in a slow, irreversible manner such that the true K_d of *Pf*AdoMetDC would be slightly elevated in the presence of DTT.

Table 3.7 lists the relative proportions of the dimer and monomeric proteins for both *Pf*AdoMetDC and the C505S mutant protein at concentrations of 1 mg/ml and 4 mg/ml as determined by analytical SEC. The apparent K_d values were found to be in the micromolar range, suggesting relatively weak propensity for dimer formation, with a higher tendency of *Pf*AdoMetDC to dimerise than the C505S mutant (K_d value 87% less than that of the mutant) (Table 3.7). The K_d value of dimeric *Pf*AdoMetDC in the absence of DTT (9.75 µM) is a 300-fold higher than the estimated K_d of 33 nM for the human protein [185], showing a comparatively reduced propensity of the plasmodial protein to dimerise. However, this K_d value for *Pf*AdoMetDC is similar to that of monomeric plant AdoMetDC (15.38 µM), its nearest conserved orthologue which has been structurally characterised [184]. Upon concentration of the *Pf*AdoMetDC-C505S mutant sample to 4 mg/ml, the K_d value decreased by 75% while the *Pf*AdoMetDC protein's constant decreased by 42% (Table 3.7). In general, the K_d values of the *Pf*AdoMetDC protein were less than the mutant, indicating that a single mutation at the dimer interface decreased the dimerisation propensity of *Pf*AdoMetDC.

Table 3.7: Dissociation constants for *Pf*AdoMetDC and the C505S mutant from analytical SEC
The relative proportions of the dimers and monomers for both the wild-type and C505S mutant *Pf*AdoMetDC proteins at two different protein concentrations were obtained from SE chromatograms and used to estimate their dissociation constants. These were then compared to the dissociation constants of the confirmed dimeric human and monomeric plant AdoMetDCs.

Sample	Concentration		X_D	X_M	[D] (µM)	[M] (µM)	K_d (µM)	K_a (μM^{-1})	Reference
	mg/ml	µM							
*Pf*AdoMetDC	1	14.65	0.53	0.42	3.88	6.15	9.75	0.1	-
	4	58.59	0.74	0.19	21.68	11.13	5.71	0.18	
*Pf*AdoMetDC-C505S	1	14.65	0.22	0.74	1.61	10.84	72.98	0.014	-
	4	58.59	0.58	0.30	16.99	17.58	18.19	0.055	
Human			-				0.033	30.3	[185]
Plant			-				15.38	0.065	[184]

The concentrations of monomer [M] and dimer [D] were calculated as follows: $[M] = [C] \times X_M$, $[D] = \frac{M_0 - [M]}{2} = \frac{[C] \times X_D}{2}$. Where M_0 is the total molar concentration, X_M and X_D are the relative proportions of monomer and dimer, and C (µM) is the protein concentration applied to the SEC column. Assuming simple monomer-dimer equilibrium in the absence of a reducing agent, the apparent dissociation constant of the dimer could then be calculated as follows: $K_a = \frac{[D]}{[M][M]} = \frac{1}{K_d}$.

3.3.4.3. Disulphide-independent dimerisation of *Pf*AdoMetDC

Despite the addition of a reducing agent and the mutagenesis of Cys505 at the proposed dimer interface of *Pf*AdoMetDC, dimerisation of the protein was still observed, which indicates the presence of an additional dimerisation-mediated process. In the absence of *Pf*ODC, dimerisation of monofunctional *Pf*AdoMetDC may be mediated by a hydrophobic patch on the *Pf*AdoMetDC protein surface, which is natively involved in an interaction with the *Pf*ODC domain within the *Pf*AdoMetDC/ODC complex. Based on extensive protein-protein docking results [152], such an interaction between two *Pf*AdoMetDC monomers would therefore occur in a side-to-side fashion involving the α-helices that flank the αββα-sandwich fold and not the proposed dimer interface that occurs as an edge-on association of the β-strands. The results of docking the *Pf*AdoMetDC domain to the *Pf*ODC domain and *vice versa*, identified the site on *Pf*AdoMetDC where *Pf*ODC is most likely to bind [152]. The *Pf*AdoMetDC residues that were predicted to interact with *Pf*ODC include Phe94, Phe98, Asp101, Phe159, Glu160, Gln161, Glu162, Tyr163, Phe174, Phe177 and Lys180 (Figure 3.9A). These residues are located on the α-helices flanking the core β-strands. In turn, the *Pf*ODC residues that are likely to interact with *Pf*AdoMetDC have also been identified (Figure 3.9B). Interestingly, the latter predicted docking site is in proximate position to the highly conserved *Pf*ODC domain O1 parasite-specific insert, which was previously shown to mediate protein-protein interactions within the bifunctional complex (Chapter 2).

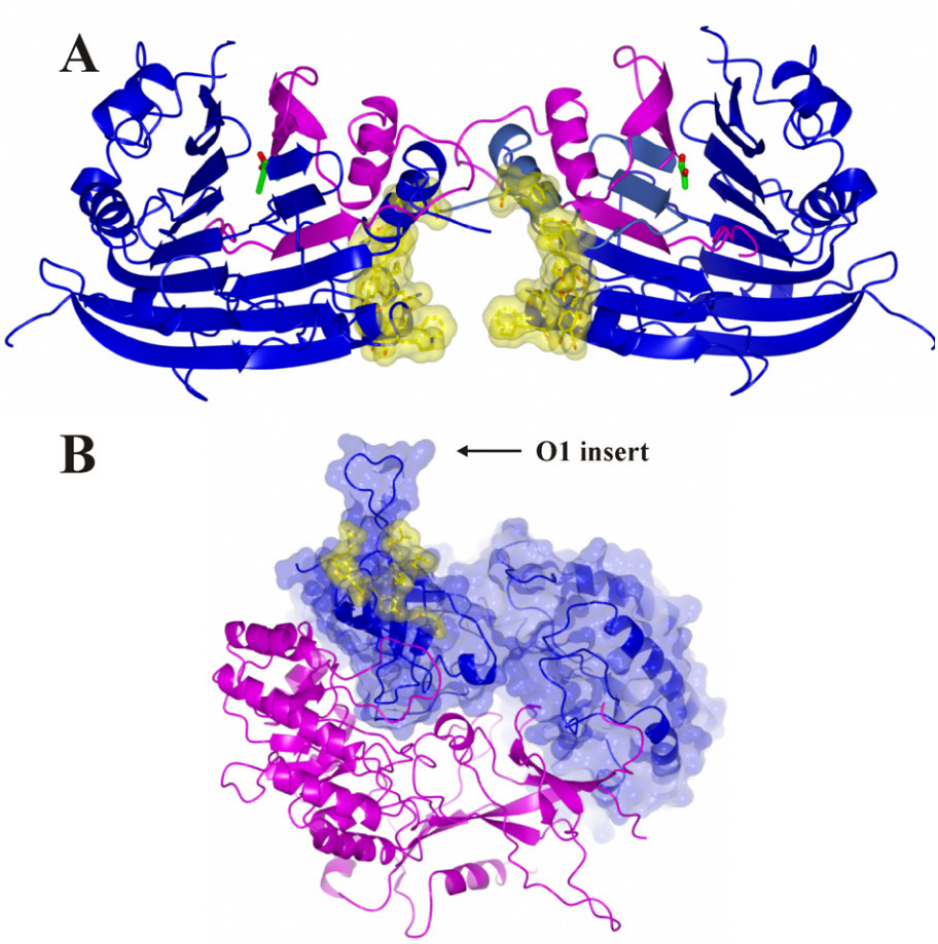

Figure 3.9: Predicted structural description of *Pf*AdoMetDC/ODC showing the proposed domain-domain interaction sites.
(A) The homology model of monomeric *Pf*AdoMetDC (β- and α-subunits shown in magenta and blue, respectively) [120] and (B) homodimeric *Pf*ODC (two monomers shown in magenta and blue) [127] are shown. The residues that are predicted to interact with the *Pf*ODC domain on the surface of *Pf*AdoMetDC and *vice versa* are shown in yellow. Two monomers of monofunctional *Pf*AdoMetDC can interact with each other in a side-to-side fashion at the site where *Pf*ODC natively interacts within the bifunctional complex. The position of the O1 parasite-specific insert is indicated. The pyruvoyl co-factors in the *Pf*AdoMetDC active sites are shown in green.

To confirm the hydrophobic-mediated interaction of the *Pf*AdoMetDC monomers, the mutant C505S protein (~6 mg/ml) was separated with SEC in wash buffer containing 10 mM DTT and 5% (v/v) n-butanol. This organic solvent was identified following the initial testing of a variety of agents at various concentrations that are known to disrupt hydrophobic interactions (results not shown). If a hydrophobic patch is exposed on the surface of *Pf*AdoMetDC the organic solvent is expected to shield this patch and thereby prevent the side-to-side interaction of the protein while DTT and the C505S mutation is expected to prevent the edge-on dimerisation via the proposed dimer interface. Figure 3.10 shows the SEC analysis of *Pf*AdoMetDC-C505S in the presence of DTT and butanol, which resulted in a single protein elution peak at 15.1 ml (V_e/V_o of 1.79) corresponding to a calculated MW of the monomeric protein 77 kDa in size. The addition of butanol therefore protected the hydrophobic patch on *Pf*AdoMetDC and constrained the protein to its monomeric form.

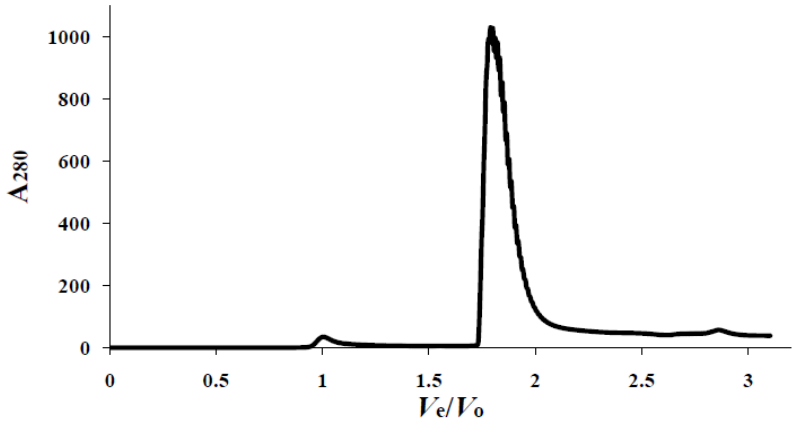

Figure 3.10: SEC of *Pf*AdoMetDC-C505S in the presence of DTT and n-butanol.
The *Pf*AdoMetDC-C505S mutant protein at a concentration of 6 mg/ml was separated with SEC on a column equilibrated with 50 mM Tris/HCl, pH 8.0, 150 mM NaCl, 10 mM DTT and 5% n-butanol.

Subsequent activity analysis of the protein collected from SEC showed that the enzyme is inactive while extensive dialysis with wash buffer recovered 65% of the activity of the butanol-treated enzyme in comparison to the untreated *Pf*AdoMetDC activity (results not shown).

3.3.5. Far-UV analyses of *Pf*AdoMetDC indicates a similar fold as the human protein

Far-UV CD was performed to determine the secondary structure of the *Pf*AdoMetDC protein (in the absence of DTT) for comparison to dimeric human AdoMetDC [185] as well as to observe any secondary structural changes that might take place in the predominantly monomeric C505S mutant protein. Prior to CD analyses, the R_H of the proteins were analysed with DLS to ensure that the Cl^--free phosphate buffer did not cause protein aggregation or affect the oligomeric state of the proteins (results not shown).

At the concentration of 0.5 mg/ml (7.2 µM) used in these analyses, mainly monomeric protein is expected based on the SEC result, however, by using the estimated K_d values that were determined for the wild-type *Pf*AdoMetDC and C505S mutant proteins (Table 3.7), the dimeric proportions within these samples were estimated to be present at 45% and 15%, respectively. The results showed that *Pf*AdoMetDC conforms to proteins with significant β-sheet content (40%), with a minimum at 209.5 nm and a maximum at 191 nm (Figure 3.11). This correlates well with what has been predicted in the homology model of *Pf*AdoMetDC [120] and dimeric human AdoMetDC, which showed a minimum at 218 nm and a maximum at 195 nm [185]. It is conceivable that parasite-specific inserts of unknown structure (constituting 32% of the 572-residue *Pf*AdoMetDC protein [120]), contribute to the differences in the spectra with 34% of the *Pf*AdoMetDC secondary structure indicated to be disordered with Far-UV CD.

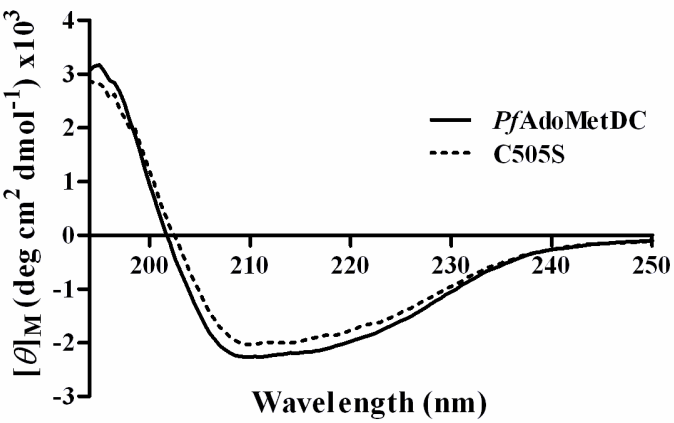

Figure 3.11: Far-UV CD analyses of the *Pf*AdoMetDC and C505S mutant proteins.
Far-UV CD analysis was performed on the *Pf*AdoMetDC and C505S mutant proteins in a phosphate buffer between wavelengths of 190 nm and 150 nm to detect possible differences in secondary structures of the mainly dimeric and mainly monomeric proteins, respectively.

The spectra of *Pf*AdoMetDC and the C505S mutant proteins are similar with minimum peaks at ~210 nm (Figure 3.11). These results provided confidence in the fact that, while the C505S mutation in *Pf*AdoMetDC stabilised the monomeric form and showed a reduced propensity of the protein to covalently dimerise, neither the mutation nor the monomeric status affected the secondary structure of the proteins.

Thus far the results have shown that monofunctional *Pf*AdoMetDC has a lower propensity than the human protein to dimerise. Furthermore, at the concentration used in the activity assays and by applying the K_d value of *Pf*AdoMetDC (Table 3.7) it can be calculated that >95% of the protein will be in its monomeric form, which implies that the protein does not require dimerisation to be functionally active. The *in vitro* conditions showed that *Pf*AdoMetDC exists as two different dimers involving two sites on the protein surface. The C505S mutant results showed that disulphide linkage enhances the formation of the dimer at the predicted dimer interface [120] and butanol treatment showed that additional dimer formation is mediated by a site that could be involved in the native interaction with the *Pf*ODC domain [152].

3.3.6. Studies of the mechanism of processing in *Pf*AdoMetDC

Processing of human and *T. cruzi* AdoMetDC is stimulated by putrescine binding in a charged-buried site distant from the active site. However, in the case of *P. falciparum* AdoMetDC, neither catalytic activity nor processing is stimulated by putrescine, which alludes to a different mechanism of processing for this protein. Heterologous expression of *Pf*AdoMetDC within *E. coli* also showed that the processing reaction is not 100% efficient (Figure 3.2A). To elucidate

the mechanism of autocatalytic processing in *Pf*AdoMetDC the residues involved in processing as well as the ones that assume the role of putrescine binding should be identified. Table 3.8 lists the residues that are predicted to be involved in the processing reactions of AdoMetDC from different organisms, which were identified with a multiple structure-based alignment of the sequences from human, plant and *Plasmodium* [120].

Table 3.8: Alignment of residues involved in the active site, processing reaction and the putrescine-binding site or charged-buried site for AdoMetDC from three organisms
Residues in the top row are numbered according to the human protein template while the residues in the bottom row are numbered according to the *P. falciparum* protein template. Residues in yellow are involved in the active site, green in the processing reaction and blue in the putrescine-binding site (*H. sapiens*) or charged-buried site (*P. falciparum* and *S. tuberosum*). Conserved residues are shown in grey.

	13	15	17	67	68	82	174	178	223	229	243	247	256
H. sapiens	L	E	W	E	S	C	D	E	F	S	H	E	E
S. tuberosum	R	E	S	E	S	C	R	E	F	S	H	E	E
P. falciparum	R	V	K	E	S	C	K	E	F	S	H	E	E
	11	13	15	72	73	87	215	219	415	421	434	438	447

Table 3.8 shows that the residues involved in the active site and processing reaction are highly conserved between the organisms, while the residues that have been shown to be involved in putrescine binding of the human protein are not well conserved and shows significant diversity. The *Pf*AdoMetDC homology model showed that three basic amino acids (Arg11, Lys15 and Lys215) occupy the regions of the acidic residues that were shown to interact with putrescine in the human crystal structure (hGlu15, hAsp174, hGlu178 and hGlu256). In *P. falciparum* these residues correspond to Val13, Lys215, Glu219 and Glu447 (Figure 3.12). Therefore, in *P. falciparum*, hGlu15 is replaced by Val13 and positively-charged residues Arg11 and Lys15 are located approximate to the position where one terminal of putrescine would be positioned while Lys215 occupies the position of the other terminal, thereby mimicking putrescine binding (Figure 3.12) [120].

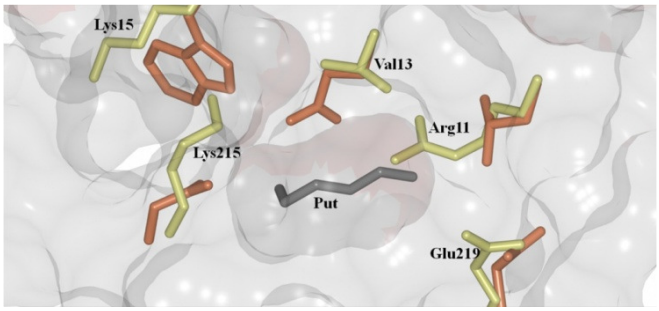

Figure 3.12: The charged-buried site of *Pf*AdoMetDC.
Putrescine in grey from the human AdoMetDC crystal structure (1I7M) is shown with the residues that are predicted to stabilise putrescine binding in orange. The corresponding residues from the *Pf*AdoMetDC homology model [120] that are predicted to mimic putrescine binding are shown in yellow. Taken from Birkholtz *et al.* (Biochemical Journal, in press).

In the current study, residues Ser421 and Arg11 were investigated for their roles in *Pf*AdoMetDC processing. Mutagenesis of the Ser421 residue (corresponding to hSer229, previously shown to be essential for processing [125]) to Ala did not prevent processing of *Pf*AdoMetDC since both the processed ~61 kDa mutant protein and the ~9 kDa dissociated β-subunit could be identified on the 12.5% acrylamide gel (Figure 3.13A and B, lane 2).

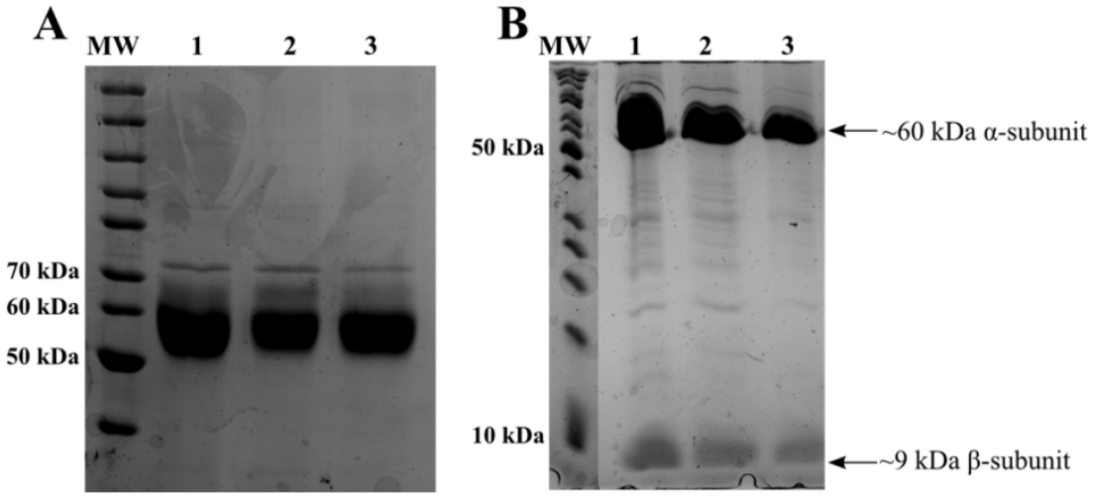

Figure 3.13: SDS-PAGE analysis of the S421A *Pf*AdoMetDC mutant protein to determine the role of this residue in autocatalytic processing.
The Ser421 residue was mutated to Ala and the expressed mutant protein was analysed with (A) 7.5% and (B) 12.5% SDS-PAGE gels in order to identify the ~60 kDa α- and ~9 kDa β-subunits as an indication of processing taking place in the *Pf*AdoMetDC protein. MW: PageRuler Unstained Protein Ladder. (A) and (B) lane 1: wild-type *Pf*AdoMetDC; lane 2: *Pf*AdoMetDC-C505S; lane 3: *Pf*AdoMetDC-S421A. The positions of the ~60 kDa α- and ~9 kDa β-subunits of *Pf*AdoMetDC are indicated with arrows.

In *T. cruzi*, it was previously shown that mutation of Arg34 in this parasite's AdoMetDC to the corresponding residue in human AdoMetDC (hLeu13) abolished processing while the crystal structure of plant AdoMetDC showed that the corresponding residue Arg18 is located at the approximate position that putrescine occupies in the human protein [184]. Similarly, in the current study Arg11 of *Pf*AdoMetDC was mutated to Leu to observe its possible role in *Pf*AdoMetDC processing. The results confirmed previous findings [120] and showed that the *Pf*AdoMetDC-R11L mutant only expressed as the unprocessed protein at ~70 kDa (Figure 3.14A, lane 1) while the ~9 kDa β-subunit could not be identified on the 12.5% acrylamide gel (Figure 3.14B, lane 1).

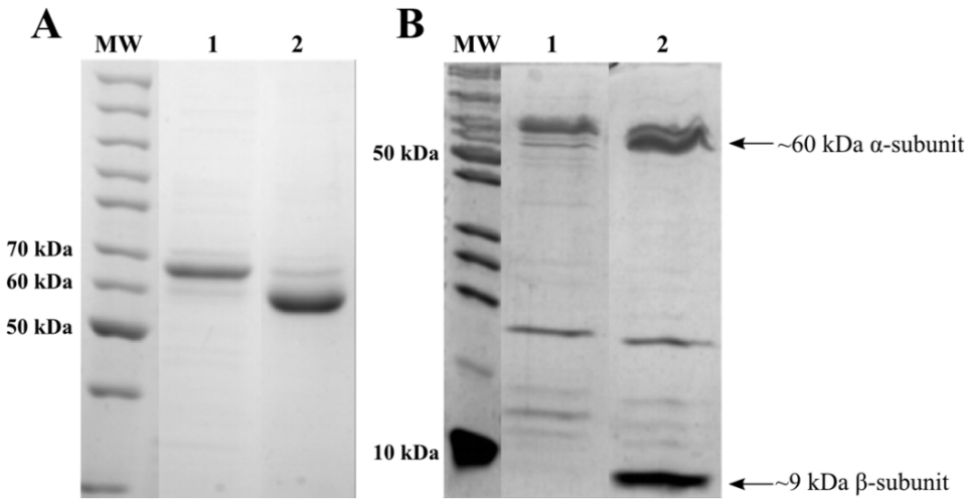

Figure 3.14: SDS-PAGE analysis of the R11L *Pf*AdoMetDC mutant protein to determine the role of this residue in autocatalytic processing.
The Arg11 residue was mutated to Leu and the expressed mutant was analysed with (A) 7.5% and (B) 12.5% SDS-PAGE gels. MW: PageRuler Unstained Protein Ladder. (A) and (B) lane 1: *Pf*AdoMetDC-R11L and lane 2: wild-type *Pf*AdoMetDC.

Subsequent activity analyses showed that although mutagenesis of the Ser421 residue did not affect processing of *Pf*AdoMetDC, enzyme activity decreased by 25% (Figure 3.15), which indicates that either the rate of the processing reaction was affected by the mutation or that the activity was disrupted due to the proximate position of Ser421 in the active site. Activity analysis of the *Pf*AdoMetDC-R11L mutant confirmed the SDS-PAGE results in Figure 3.14 since the mutant enzyme showed no activity indicating complete disruption of processing (Figure 3.15).

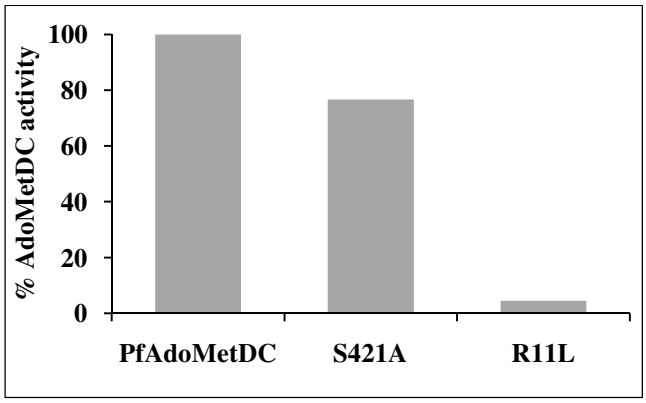

Figure 3.15: Activity analyses of the S421A and R11L *Pf*AdoMetDC mutant enzymes.
The specific activities in nmol/min/mg were normalised to the wild-type protein activity and expressed as a percentage. The results were determined from a single experiment (n=1) carried out in duplicate.

3.3.7. Enzyme kinetics of monofunctional *Pf*AdoMetDC

Since the oligomeric status of the active, mainly monomeric, monofunctional *Pf*AdoMetDC protein that was expressed from a codon-harmonised construct has now been established and the secondary structure as well as mechanism of autocatalytic processing has been investigated, the

enzyme kinetics of this protein was repeated for comparison to that of other AdoMetDCs. Typical Michaelis-Menten kinetics was observed (Figure 3.16A) and linear transformation of the Michaelis-Menten equation with the Hanes-Woolf plot [198] resulted in a K_m of 250 µM and a V_{max} of 77 nmol/min/mg for *Pf*AdoMetDC (Figure 3.18B). The K_m calculated here for *Pf*AdoMetDC is approximately 4-fold higher than reported for the 660-residue wt*Pf*AdoMetDC-hinge enzyme and approximately 6-fold higher when *Pf*AdoMetDC is associated with *Pf*ODC in the bifunctional complex (Table 3.9) [71]. However, the K_m determined here is in a similar range to that of the homodimeric trypanosomal AdoMetDC orthologues (Table 3.9).

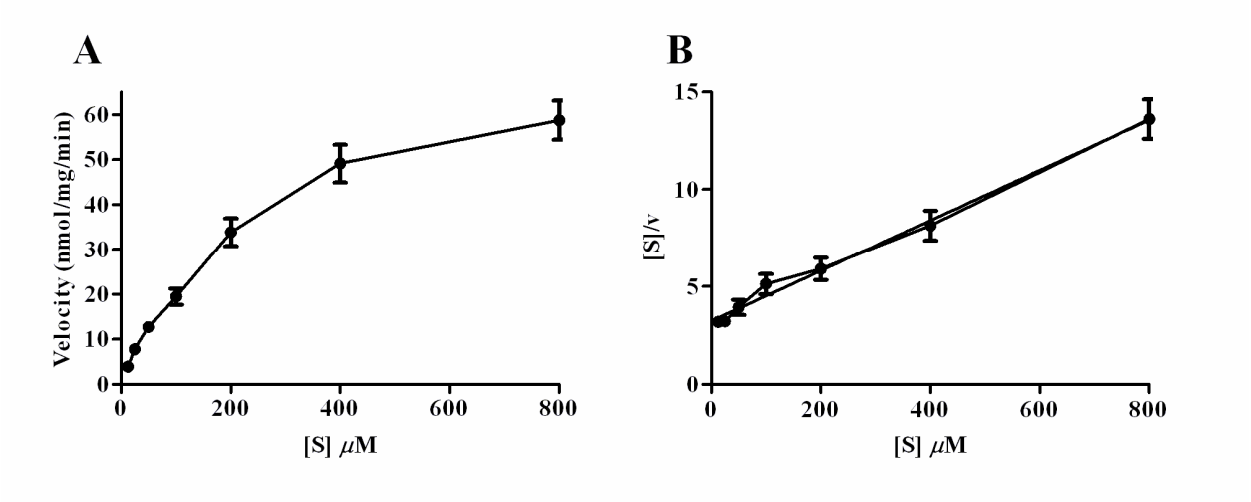

Figure 3.16: Michaelis-Menten curve (A) and linear Hanes-Woolf plot (B) of *Pf*AdoMetDC reaction velocity measured at different substrate concentrations.
(A) The substrate affinity constant as well as V_{max} of *Pf*AdoMetDC was determined using Michaelis-Menten kinetics. A substrate dilution series ([S]) ranging from 12.5 to 800 µM was used to determine the mean of the reaction velocities (v, nmol/mg/min) from three independent experiments carried out in duplicate. S.E.M is indicated. (B) The linear Hanes-Woolf plot was subsequently used to determine the K_m and V_{max} values.

The k_{cat} of *Pf*AdoMetDC was calculated to be 5.3 min^{-1}, the enzyme therefore converts a molecule of substrate into product in approximately 11 s compared to the 0.4 s it takes for human AdoMetDC (Table 3.9). The k_{cat} values of the wt*Pf*AdoMetDC-hinge and the bifunctional protein preparation of *Pf*AdoMetDC are similar and in the range of 3.3 to 4 min^{-1} (Table 3.9). The specificity constant (k_{cat}/K_m) for *Pf*AdoMetDC was calculated to be 332 $M^{-1}s^{-1}$. This value is 3- to 4-fold less than previously reported [71] and is the lowest of the proteins analysed (Table 3.9).

Thus, it appears that the presence of the hinge region (and/or *Pf*ODC) in some way improves the kinetics of *Pf*AdoMetDC by increasing its substrate affinity. Importantly, compared to previous findings [71] a similar trend is observed in which monofunctional *Pf*AdoMetDC shows less catalytic efficiency as indicated by the k_{cat} and K_m values compared to when the protein is in complex with *Pf*ODC.

Table 3.9: Comparison of enzyme kinetics for AdoMetDC from different organisms

The enzyme kinetics of *Pf*ODC are also included in order to show how the K_m and k_{cat} values of the monofunctional enzymes change when they become associated with the neighbouring domain of the bifunctional *Pf*AdoMetDC/ODC complex.

Organism	Protein arrangement, oligomeric state	K_m [a]	K_m [a] +put	k_{cat} (min^{-1})	MDL73811	CGP48664 [b]	Putrescine effect	Reference
H. sapiens	Homodimer	74	59	114 (-put) 156 (+put)	0.56	5000 (-put) 0.005 (+put)	Stimulates activity and processing	[186,204,205]
P. falciparum	Monofunctional *Pf*AdoMetDC, monomer	250	-	5.4	0.33	4.1	No effect	Current study
	Monofunctional *Pf*AdoMetDC-hinge	58		4	-	3		[71,100]
	Bifunctional *Pf*AdoMetDC/ODC, heterotetramer	43		3.3	1.6	-		[71,100]
T. cruzi	Homodimer	260	250	-	-	100 (-put) 6 (+put)	Stimulates activity of homo- and heterodimer	[186]
	Homodimer	540	130	0.3 (-put) 1.44 (+put)	-	-		[164]
	Monomer/prozyme, heterodimer	580	170	36 (-put) 50.4 (+put)	-	-		[164]
T. brucei	Homodimer	380	240	0.096 (-put) 0.492 (+put)	-	0.49	Stimulates activity of homodimer	[164,206]
	Monomer/prozyme, heterodimer	110	170	84 (-put) 102 (+put)	-	-		[164]

[a] The K_m values (in µM) are given in the presence and absence of putrescine (put) in the organisms where putrescine stimulates the activity of the protein.
[b] The K_i values (in µM) are given in the presence and absence of putrescine (put) in the organisms where putrescine stimulates the activity of AdoMetDC.

Analysis of enzyme kinetics in the presence of the irreversible inhibitor MDL73811 showed that *Pf*AdoMetDC activity decreased in a concentration dependent manner (Figure 3.17A). A secondary plot yielded a linear graph from which a k_{inact} value of 0.46 min^{-1} and a K_i value of 0.33 µM were determined for MDL73811 (Figure 3.17B). Comparison to the reported K_i of 1.6 µM for MDL73811 on *Pf*AdoMetDC/ODC [100] indicates stronger inhibition of the monofunctional enzyme (Table 3.9).

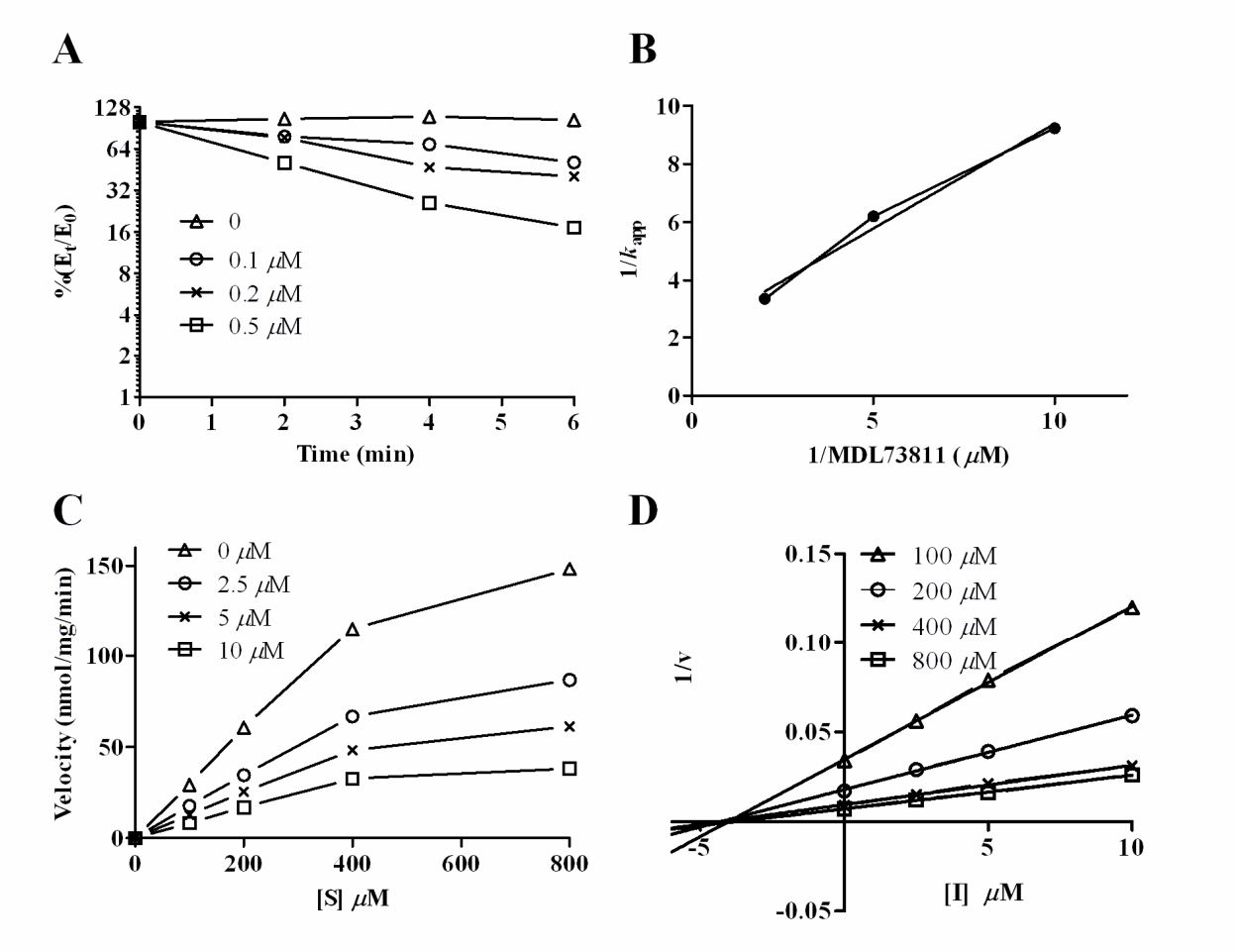

Figure 3.17: Inhibition kinetics of *Pf*AdoMetDC treated with MDL73811 and CGP48664.
For the irreversible inhibitor MDL73811 the Kitz-Wilson method was used where the percentage enzyme activity (given by the maximal enzyme activity following pre-incubation with a specific [I]) for time interval t (E_t) over the enzyme activity following pre-incubation in the absence of inhibitor for each [I] tested (E_0)) against time is shown (A). Linearisation was performed by plotting the inverse of the slope from the primary plot versus the inverse of [I]. For inhibition with CGP48664 the Michaelis-Menten curves (C) showing the reaction velocities (v, nmol/mg/min) in the presence of a substrate ([S]) dilution series ranging from 100 µM to 800 µM and an inhibitor dilution series ranging from 2.5 µM to 10 µM are indicated. The linear Dixon plots (D) were obtained by plotting the inverse of the reaction velocities against [I].

Inhibition kinetics of *Pf*AdoMetDC with the CGP48664 showed that increasing concentrations of CGP48664 did not affect the K_m of *Pf*AdoMetDC but instead decreased the V_{max}, which is typical of a non-competitive inhibitor whereby binding of the native substrate is not affected (constant K_m) but the efficiency of the reaction is decreased (Figure 3.17C). Linearisation of the

Michaelis-Menten curves resulted in a K_i of 4.1 µM (Figure 3.17D), which is similar to the reported value for wt*Pf*AdoMetDC-hinge (Table 3.9) [100]. The finding that the inhibition of *Pf*AdoMetDC by CGP48664 is non-competitive is similar to that observed for *T. cruzi* AdoMetDC [186]. In contrast, the inhibition of human AdoMetDC with CGP48664 is competitive [124].

3.4. Discussion

The polyamine biosynthetic activities of *P. falciparum* are uniquely arranged on a bifunctional *Pf*AdoMetDC/ODC protein consisting of 1419 residues of which the hinge region is predicted to be encoded by residues 530-804 [71]. The evolutionary role of such a large complex has been extensively questioned. A possible reason could be the combined regulation of two enzymes in a pathway via the interference of a single domain, which then communicates the change to the adjacent domain. Another unique property of *Pf*AdoMetDC/ODC is the presence of five parasite-specific inserts that range in size between 6 and 157 residues and are located within both the *Pf*AdoMetDC [120] and *Pf*ODC [127] domains. Possible roles for these inserts, with unknown structure, in interdomain interactions mediating activity have been shown [69]. In this study, various biochemical and structural characteristics of the monofunctional *Pf*AdoMetDC domain was investigated to provide an understanding of this protein's functionality as a monofunctional protein compared to its role within the bifunctional complex. This information would provide us with novel insights into the possible role of the bifunctional complex in the homeostatic maintenance of polyamine levels within *P. falciparum* parasites.

Homology modeling of the *Pf*AdoMetDC monomer with the plant structure as template predicted the same four-layer αββα-sandwich fold [120] as was observed with the human and plant AdoMetDCs [123,184]. Furthermore, the active site and charged-buried site residues of *Pf*AdoMetDC are conserved with similar conformation to that of the human counterpart. In contrast to *Pf*AdoMetDC, which does not bind putrescine [71], the crystal structure of human AdoMetDC revealed the presence of an unusual collection of charged residues between the β-sheets of each monomer that binds putrescine in a positively cooperative manner [125,185,189,207]. The functional oligomeric unit of *Pf*AdoMetDC has not been elucidated but since this protein does not bind putrescine, dimerisation of *Pf*AdoMetDC is not expected to have a functional role. This is according to the postulation by Bale *et al.* in a study of human AdoMetDC where they showed that putrescine binding and dimerisation may be linked resulting

in positive cooperativity between the monomers of the human protein [185]. The lack of information on the biochemical characteristics of *Pf*AdoMetDC could be ascribed to the ineffective heterologous expression of soluble forms of plasmodial proteins [208] such as *Pf*AdoMetDC/ODC

In this study, codon harmonisation of the monofunctional *PfAdometdc* gene was carried out to test whether this technique could improve the heterologous protein expression within *E. coli*. Codon harmonisation looks at the frequency of codon usage for each amino acid in *P. falciparum* and their preference in *E. coli*, and then alters the code of the gene to the codon frequency of the non-natural host (*E. coli*) [209]. In contrast to codon optimisation, these changes thus ensure that the positional codon frequency of low/intermediate and high usage codons remain similar in the non-natural host, which then allows the speed of translation to match that of the natural host. Assuming that the translational machineries of the expression and natural host organisms are similar, translation and pausing at the particular sites where folding of the secondary and tertiary structures are required, is expected to occur as it would occur in the natural host. Additionally, any false Shine-Dalgarno sites are removed that may result in the truncation of the proteins within the expression host.

Comparison of the expression of the wt*Pf*AdoMetDC-hinge and *Pf*AdoMetDC proteins encoded from wild-type, unharmonised and harmonised sequences, respectively, showed that harmonisation improved the expression levels as well as protein stability of monofunctional *Pf*AdoMetDC. The reduction of Hsp70 co-purification in the *Pf*AdoMetDC sample also gives an indication that less pressure was placed on *E. coli* during protein translation and folding. However, the possible improvement of protein expression due to the removal of the Strep-tag at the N-terminus of *Pf*AdoMetDC cannot be excluded. Addition of unharmonised nucleotides to the harmonised gene to produce a protein comparable in size to that of wt*Pf*AdoMetDC-hinge (residues 1-660) [71] did not result in soluble protein. The hinge region may therefore affect soluble protein expression. Furthermore, soluble expression of *Pf*AdoMetDC within *E. coli* showed the presence of both the unprocessed and processed proteins after affinity chromatography indicating that the heterologous expression prevented the 100% efficiency of the processing reaction. These results show that folding of the protein was not optimal to allow the correct positioning of the residues involved in the autocatalytic cleavage reaction. Subsequent analysis of the insoluble protein extracts showed that a considerable amount of these proteins were expressed as insoluble inclusion bodies. Refolding and purification of

monofunctional *Pf*AdoMetDC from the insoluble inclusion bodies was therefore performed, firstly in an attempt to increase the yield and purity of the protein and secondly to determine if correct refolding under favourable *in vitro* conditions could lead to increased processing efficiency since it is generally accepted that simply the correct structural conformation of *Pf*AdoMetDC is required for pyruvoyl co-factor formation. The results showed that even though significant amounts of pure protein (without Hsp70 contamination) could be obtained from the inclusion bodies, processing of both the *Pf*AdoMetDC and *Pf*AdoMetDC-hinge proteins were abolished and only resulted in the isolation of inactive, unprocessed proteins. Preliminary far-UV CD analyses of these samples showed similar overall secondary structural content compared to the proteins isolated from the soluble fraction but the conformation of the proteins are unknown.

Prior to the investigative experiments to determine the oligomeric structure and activity of the soluble *Pf*AdoMetDC protein, different buffer screens were tested with DSF to ensure the stability of the protein. DSF identifies ideal buffer solutions, low molecular weight ligands or protein-inhibitor/substrate complexes that could contribute to protein stabilisation. In the presence of the SYPRO orange dye the protein's Tm corresponds to the temperature at which there exists an equivalent concentration of folded and unfolded proteins. If the stability of a protein is subsequently increased as a consequence of, for example, the co-incubation of substrate, the free energy contribution of substrate binding results in an increase in the temperature at which this equilibrium is obtained, which is consequently shown by an increase in the protein's Tm [193]. In this study, DSF analyses showed that, in comparison to a whole range of buffers that were tested, the stability of *Pf*AdoMetDC in dialysis buffer consisting of 50 mM Tris/HCl, pH 8.0 and 150 mM NaCl was similar to the Tm obtained in the buffer that stabilised the protein the most. Co-incubation of the protein with substrate analogues also resulted in further increases of *Pf*AdoMetDC stability.

Investigations into the oligomer formation of *Pf*AdoMetDC were performed using SEC, non-reducing SDS-PAGE and DLS on a pure, stable form of the protein expressed from a harmonised gene. A concentration-dependent monomer-dimer equilibrium exists for the *Pf*AdoMetDC protein that could be shifted towards the monomeric form when reducing conditions were applied. Subsequent inspection of the equivalent human AdoMetDC dimer interface in the *Pf*AdoMetDC model [120] suggested the involvement of the Cys505 residue in disulphide bond formation between two monomeric proteins. This residue is not conserved amongst all AdoMetDCs but since it is located on the β15 strand at the proposed dimer interface,

it could form a disulphide bond with the same residue from a second monomer and thereby stabilise the dimeric form under oxidising conditions. This residue was subsequently mutated since it was predicted that if the *Pf*AdoMetDC protein dimerises at the same dimer interface as the human protein, even if this occurs at a lower association constant, then both the *Pf*AdoMetDC and Cys505 mutant proteins are expected to show dimeric forms with SEC. However, if the Cys505 residue does lie at the dimer interface and stabilises the dimeric form of the protein via disulphide bond formation, then the wild-type and mutant proteins would probably show different dimer propensities. Mutagenesis of Cys505 confirmed the modelling predictions and MALDI-MS results, which showed that Cys505 is indeed located at the native dimer interface since the mutant form reduced the propensity of *Pf*AdoMetDC to dimerise (~7.5-fold increase in K_d).

The K_d of *Pf*AdoMetDC in the low micromolar range indicated that this protein forms a much less stable dimer, which is 300-fold higher than that of the dimeric human protein [185] but similar to the monomeric plant protein [184]. DLS results also showed that mutation of Cys505 shifted the dimer-monomer equilibrium of *Pf*AdoMetDC towards the monomer and treatment of *Pf*AdoMetDC with a reducing agent immediately prior to DLS analysis was not as effective as this mutation in decreasing unwanted oligomer formation even at a concentration of the mutant protein double than the wild-type. The results show that while *Pf*AdoMetDC forms a dimer that involves the same dimer interface as the human protein, dimerisation occurs at a much lower affinity and is stabilised *in vitro* by a disulphide bond across the dimer interface. It should also be noted that the formation of the disulphide bond mediated by Cys505 is not proposed to be essential for *Pf*AdoMetDC quaternary structure formation or activity. *Pf*AdoMetDC is a cytosolic protein and due to the presence of glutathione and thioredoxin redox systems in the cytoplasm it is unlikely that the protein will be in an oxidising environment to allow the formation of a disulphide bond *in vivo* [210]. Furthermore, even though the human AdoMetDC protein is predicted to be a dimer joined by an edge-on association of the β-sheets of each monomer at the dimer interface, inspection of the 1I7M structure shows that a distance of 4.27 Å exists between the C_β atoms of the hCys148 residues on strands β7 of each monomeric protein, which could also result in the formation of a disulphide bond. The protein was, however, crystallised in the presence of 10 mM DTT [124].

Despite the prevention of disulphide bond formation at the dimer interface with the Cys505 mutation or addition of a reducing agent, SEC analyses showed that *Pf*AdoMetDC still formed

dimers, especially at moderately high protein concentrations. Dimerisation *in vitro* could additionally occur on a surface of the *Pf*AdoMetDC domain which is natively involved in an interaction with the *Pf*ODC domain within the bifunctional complex [69]. Protein-protein docking also identified the site on *Pf*AdoMetDC where *Pf*ODC is most likely to bind [152] and involves the α-helices flanking the core β-strands of *Pf*AdoMetDC. Such an interaction between two *Pf*AdoMetDC monomers would therefore occur in a side-to-side fashion as opposed to the edge-on association of the β-strands at the dimer interface as seen for human AdoMetDC (Figure 3.9). In addition, since the relative positions of the parasite-specific inserts in the quaternary structure of *Pf*AdoMetDC are unknown [120] their potential role in causing dimerisation and perhaps tetramerisation via hydrophobic/philic interactions cannot be excluded. Considering the site of the *Pf*AdoMetDC interaction on the *Pf*ODC domain, the O1 insert is positioned such that it could form a possible interaction with *Pf*AdoMetDC, which substantiates the results obtained in Chapter 2. However, since the C505S mutant has a significantly lower dimer affinity than the wild type, we could show here that *Pf*AdoMetDC is able to dimerise at the same site which usually mediates dimerisation of the human protein [120] and thus more closely resembles the native conformation but is not essential for activity.

Figure 3.18 summarises the proposed *in vitro* model of monofunctional *Pf*AdoMetDC oligomer formation as obtained from the results in this chapter. The inactive protomer which has not undergone autocatalytic processing was obtained with the heterologous expression of the protein as well as with protein refolding from insoluble inclusion bodies. Subsequent processing of this protomer to generate the pyruvoyl co-factor at Ser73 within the active site resulted in the formation of the α- and β-subunits which associates into the αβ-monomer. These subunits could be resolved with SDS-PAGE and were catalytically active. The αβ-monomer was shown with SEC to exist in equilibrium with an $(\alpha\beta)_2$-dimer, which is similar to that of homodimeric human AdoMetDC since dimer formation takes place as an extension of the β-sheets mediated by edge-on interactions between the β-strands from each monomer. This dimer was additionally shown to be stabilised *in vitro* via disulphide formation between the Cys505 residues from each monomer. The calculated dimerisation constant of the C505S mutant protein confirmed the location of this residue on the β-sheet at the predicted dimer interface since mutation increased the dissociation constant 7.5-fold. Oligomerisation of monofunctional *Pf*AdoMetDC, in the absence of *Pf*ODC, was also predicted to occur as a result of hydrophobic interactions at the native *Pf*ODC binding site, which involve the α-helices on the "sides" of the monomers. The inclusion of butanol during SEC of the *Pf*AdoMetDC-C505S protein confirmed that hydrophobic sites were protected

by this organic solvent resulting in the presence of the monomeric form of the protein. Higher oligomers were also shown to occur with SEC, which could form as a result of hydrophobic association and/or dimer-interface mediated interactions.

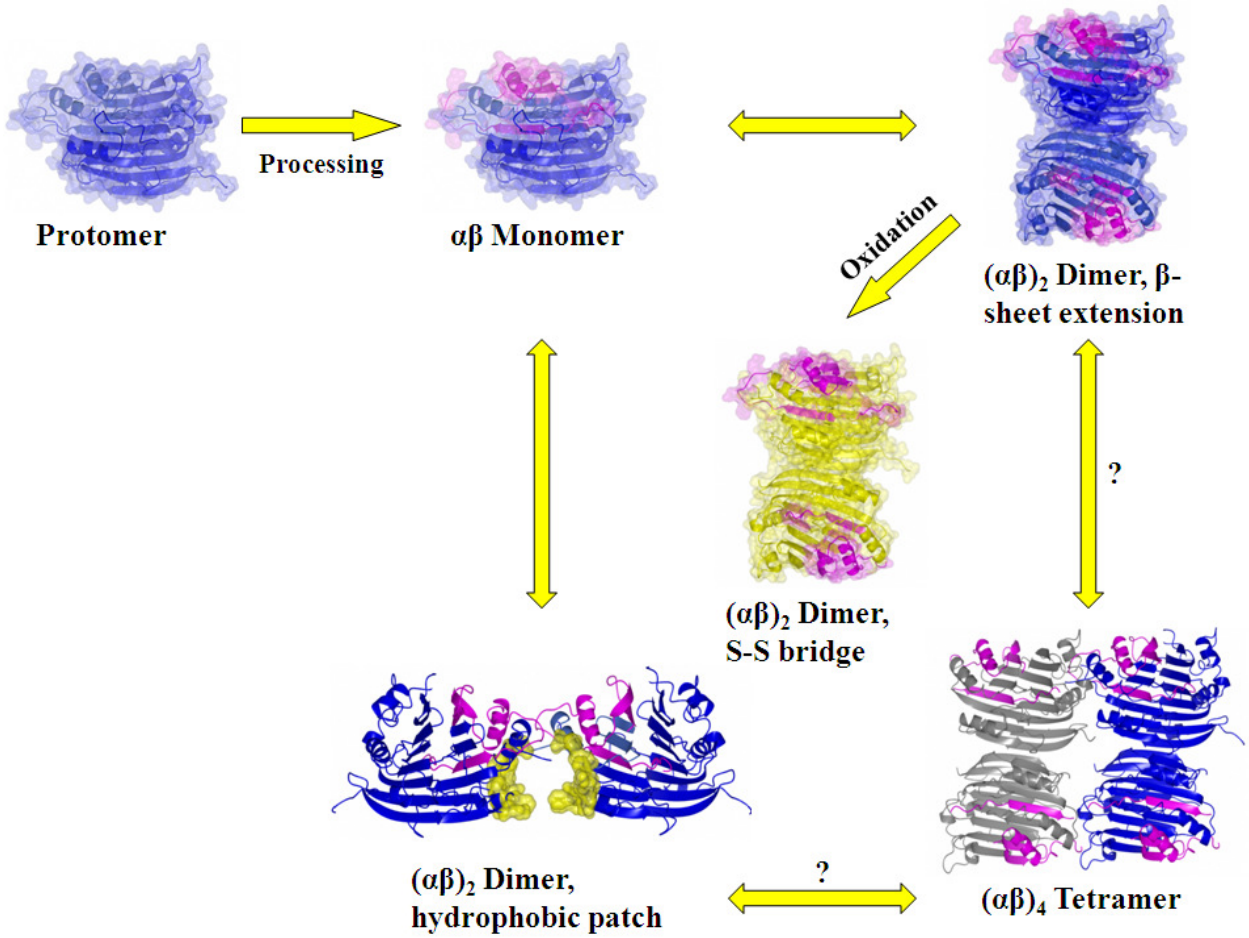

Figure 3.18: Model of monofunctional *Pf*AdoMetDC oligomerisation *in vitro*.
The protomer in blue undergoes autocatalytic processing to generate the pyruvoyl co-factor at Ser73 within the active site. Processing also forms the α- and β-subunits shown in blue and magenta, respectively, resulting in an αβ-monomer. These monomers are in equilibrium with an $(\alpha\beta)_2$-dimer, which is similar to that of homodimeric human AdoMetDC where dimer formation takes place as an extension of the β-sheets mediated by edge-on interactions between the β-strands from each monomer. Under oxidising conditions the *Pf*AdoMetDC dimer is further stabilised by disulphide bond formation between the CysC505 residues from each monomer (α- and β-subunits shown in yellow and pink, respectively) on the β-sheets at the predicted dimer interface. Oligomerisation of monofunctional *Pf*AdoMetDC, in the absence of *Pf*ODC, as a result of hydrophobic interactions at the native *Pf*ODC binding site (shown in yellow), can also occur and involve the α-helices on the "sides" of the monomers. Higher oligomers could also be formed due to hydrophobic association and/or dimer-interface mediated interactions.

Far-UV CD analyses was performed to obtain initial information on the fold of *Pf*AdoMetDC and to additionally determine whether the C505S mutation affected the structure of the protein. However, the prevention of disulphide bond formation at the dimer interface should not affect the folding properties of the protein and such a bond would only be detected in the near-UV range. The CD results showed that the AdoMetDC proteins from human and *P. falciparum* give similar spectra, with high contents of β-strands. Additionally, 30-40% of the *Pf*AdoMetDC

protein was calculated to be unordered structures and may be contributed by the parasite-specific inserts [120]. The far-UV CD analyses also confirmed identical spectra between *Pf*AdoMetDC and the mainly monomeric C505S mutant, indicating that the prevention of covalently-linked dimer association did not cause a secondary structure change in the monomeric protein.

The recombinant monofunctional *Pf*AdoMetDC protein produced here from a harmonised gene is therefore believed to be similar in conformation to the native protein. This is based on the secondary structure comparison as determined with far-UV CD that showed similarities between the *P. falciparum* and human AdoMetDCs as well as the confirmation that disulphide formation at the proposed dimer interface is mediated between closely situated Cys505 residues, which confirm the dimer interface predictions of Wells *et al*. [120]. The presence of the processed form of the recombinant protein, which is reliant on the exact positioning of the Arg11-Lys15-Lys215 triad, also indicates the correct conformation of the recombinant protein.

The mechanism of processing within AdoMetDC where a Ser residue undergoes serinolysis to produce the pyruvoyl co-factor has been extensively studied in the human and *T. cruzi* proteins where specific residues involved have been mutated and tested for their role in the processing reaction [125,185-189]. As mentioned previously, neither the catalytic activity nor processing of *P. falciparum* and plant AdoMetDC, is stimulated by putrescine. These two orthologues may therefore be constitutively processed to allow for continuously active protein, which is nonsensical in the case of plant AdoMetDC due to the various important functions that the polyamines mediate. Additionally plant AdoMetDC translation is also regulated by a well-characterised small upstream open reading frame [211,212]. For *Pf*AdoMetDC, the activity may be regulated by a different mechanism. It is also important to note that dcAdoMet is exclusively used as a substrate in the polyamine pathway, thus once produced it is committed to this pathway. It is therefore unlikely that *Pf*AdoMetDC would be constitutively active to continuously supply dcAdoMet. Moreover due to the important roles of AdoMet in various methylation reactions its abundance would be tightly regulated [178]. The expression of the constitutively active protein may therefore be regulated, which, once again, alludes to the bifunctional arrangement of *Pf*AdoMetDC and its contribution to protein activities. Furthermore the roles of AdoMet or dcAdoMet as possible allosteric effectors need to be investigated.

In *Pf*AdoMetDC, Ser73 is converted into a pyruvoyl group and previous studies have shown that mutation of this residue results in an inactive protein [71]. Residues involved in the active and

charged-buried site are conserved while those involved in putrescine-binding (human) and the charged-buried site (plant and *P. falciparum*) are diverse (Table 3.8). The *Pf*AdoMetDC homology model showed that residues Arg11, Lys15 and Lys215 may mimic putrescine binding as their locations correspond to the positions of the amino terminals of putrescine [120]. Furthermore, for human AdoMetDC, residue hSer229 was shown to be situated close to the processing site and the hydroxyl group of this residue was shown to be essential for the processing reaction as confirmed with mutagenesis and subsequent 3D structure analysis [125]. In the current study, the corresponding Ser421 residue was mutated to Ala, however, the results showed that this residue has no effect on the processing reaction but its mutagenesis resulted in decreased enzyme activity. These results show that in the parasite an alternative mechanism is involved where another residue provides the hydroxyl group needed for processing but similarly to the human protein, Ser421 does influence enzyme activity, probably due to its proximate location to the active site. This result was unexpected and indicated that differences exist between the processing mechanisms of human and *P. falciparum* AdoMetDCs that needs to be investigated further.

Previously it was shown that residues Arg34 and Arg18 from *T. cruzi* and plant AdoMetDC, respectively, are essential for processing to occur [184,187]. Arg34 represents the key structural change to explain why *T. cruzi* AdoMetDC processing is not stimulated by putrescine. In this study, the corresponding residue Arg11 from *Pf*AdoMetDC was also shown to be essential for the processing reaction [120]. These results did not only confirm the importance of Arg11 in the *Pf*AdoMetDC processing reaction but also showed that expression of such a mutant protein results in the production of a single *Pf*AdoMetDC species instead of the heterogeneous mixture of processed and unprocessed proteins obtained with wild-type protein expression. This protein, despite it being inactive, could be advantageous for future crystallisation studies in which a homogeneous protein solution is required.

This study has therefore shown that monofunctional *Pf*AdoMetDC forms a dimer in solution and that dimerisation is stabilised by various factors. More information could also be obtained on the structure as well as the unique mechanism of processing of this protein. However, since the major aim of this study was to characterise *Pf*AdoMetDC in order to obtain insights into the contribution of this domain to the bifunctional complex, enzyme kinetics of the monofunctional domain were compared to the kinetics of *Pf*AdoMetDC within the bifunctional complex. Previous studies have shown increased substrate affinity of *Pf*AdoMetDC within the bifunctional

complex [71], which is hypothesised to be introduced by subtle changes as a result of interdomain protein interactions with the *Pf*ODC domain. In Chapter 2 this was further investigated whereby the critical role of the O1 parasite-specific insert was implicated in these interactions. In this study, initial activity analyses of monofunctional *Pf*AdoMetDC reinforced previous studies [69,71], which showed that both the hinge region and the *Pf*ODC domain play important roles in the kinetic properties of *Pf*AdoMetDC. Previous studies have shown that the removal of a central part of the hinge region (residues 573-752) from the bifunctional protein decreases *Pf*AdoMetDC activity by 24% relative to its activity within the bifunctional complex [69]. Further removal of both the *Pf*ODC domain as well as half of the hinge region to create the wt*Pf*AdoMetDC-hinge protein (660 residues) increased activity by 20% [71] while, as shown in this study, the further deletion of 88 residues from the hinge region (572 residues) increased activity by 55% relative to the activity within the bifunctional complex (Figure 3.19). However, the kinetics analyses showed reduced substrate affinity of the latter enzyme (K_m of 250 µM) compared to that of the *Pf*AdoMetDC domain in the bifunctional complex (K_m of 43 µM) (Figure 3.19) [71]. The K_m value obtained here is surprisingly similar to that of homodimeric trypanosomal AdoMetDC (Table 3.9) suggesting that, in the absence of the hinge or the *Pf*ODC domain, monofunctional *Pf*AdoMetDC behaves like kinetoplastid AdoMetDCs. However, *Pf*AdoMetDC is still a less catalytically efficient enzyme compared to AdoMetDCs that are activated by putrescine (human, *T. cruzi*) or prozyme (kinetoplastids). In the presence of prozyme the k_{cat} of *T. brucei* AdoMetDC is increased 1200-fold [163] while a similar situation was seen for *T. cruzi* where both prozyme and putrescine increased the enzyme efficiency to a level similar to that of the fully activated counterpart in *T. brucei* (Table 3.9) [164]. Therefore, it can be postulated that the bifunctionallity of *Pf*AdoMetDC/ODC allows the parasite to mediate regulatory mechanisms between the two decarboxylase domains but an allosteric effector remains to be identified that could increase the enzyme efficiency of *Pf*AdoMetDC to the levels observed for human and heterodimeric trypanosomal AdoMetDCs.

The results show that binding of *Pf*ODC results in a 6-fold change in both the specific activity and K_m of *Pf*AdoMetDC resulting in slightly lower enzyme efficiency (k_{cat} of 5.3 min^{-1} versus 3.3 min^{-1}) (Figure 3.19). The K_m of monofunctional *Pf*AdoMetDC is therefore considerably increased so as to prevent the binding of metabolically important AdoMet when putrescine-producing *Pf*ODC is absent. Within the bifunctional complex, the affinities of both enzymes for their respective substrates improve (43 µM for *Pf*AdoMetDC and 42 µM for *Pf*ODC) with synchronised enzyme catalytic rates of approximately 3 min^{-1} (Figure 3.19) [71] producing

dcAdoMet and putrescine every 18-20 s for the subsequent synthesis of spermidine by *Pf*SpdS. These property changes of the two enzymes in the bifunctional complex is hypothesised to be due to subtle changes in the active site centre induced by long-range effects [134] modulated by interdomain protein interactions with *Pf*ODC [69] to regulate the polyamine levels within the parasite.

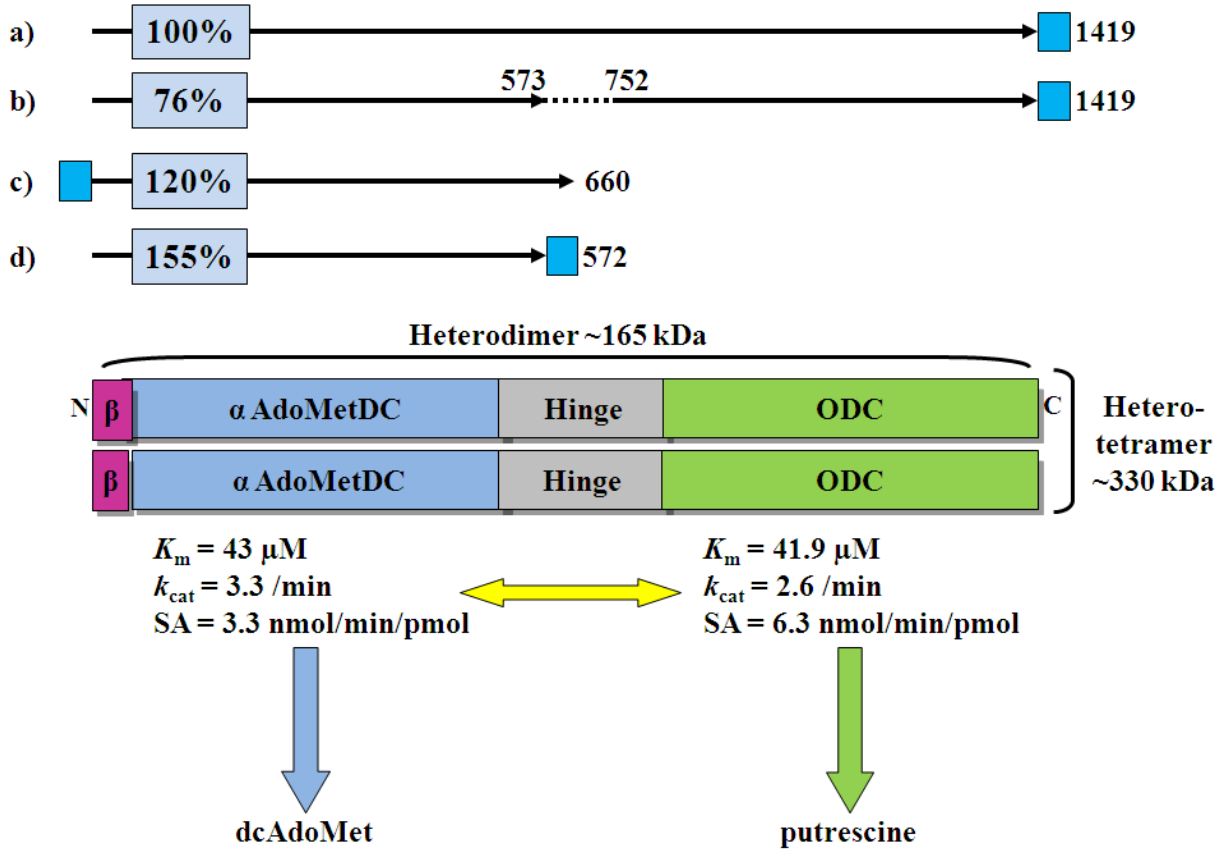

Figure 3.19: Schematic diagram describing the coordinated activities of the domains within the bifunctional AdoMetDC/ODC complex from *P. falciparum*.
In the central diagram, the *Pf*AdoMetDC/ODC bifunctional arrangement is shown with the processed α- and β-subunits of *Pf*AdoMetDC shown in blue and magenta, respectively. This domain is linked to the C-terminal *Pf*ODC domain (green) with the hinge region (grey). The approximate protein sizes of the heterodimeric complex (~165 kDa) as well as the heterotetrameric bifunctional complex (~330 kDa) are indicated [70]. Above the diagram the activities of the different constructs of *Pf*AdoMetDC are shown, which are expressed as a percentage of the *Pf*AdoMetDC activity in the bifunctional complex (a) [71] by taking into account the different sizes of the proteins in relation to the 1419-residue bifunctional protein. The lengths of the proteins are indicated as black lines in proportion to the schematic diagram of the bifunctional protein while the deleted hinge region in (b) is shown with a dashed line. The positions of the Strep-tags are shown as blue boxes. The AdoMetDC and ODC reactions produce dcAdoMet and putrescine, respectively, and enzyme kinetics have shown that within the bifunctional complex these domain activities are coordinated such that equimolar quantities of the products are synthesised. The activities of (a) and (c) as well as the enzyme kinetics data were obtained from [71], the activity of the hinge deletion mutant is from [69] while the result of the shortest protein was obtain in the current study.

Trypanosomal AdoMetDC behaviour was also observed when *Pf*AdoMetDC was treated with CGP48664. In contrast to what was shown for human AdoMetDC [124], this substrate analogue inhibited *Pf*AdoMetDC non-competitively. Similarly, non-competitive inhibition was also shown

for *T. cruzi* AdoMetDC [186] where enzyme activity was actually increased in the presence of <10 µM CGP48664 while inhibition was only observed at higher concentrations or in the presence of putrescine (K_i of 6 µM). The authors suggested that in the absence of putrescine, the compound binds to the putrescine-binding site and acts as an agonist of activity as putrescine would and when bound to the active site it acts as an inhibitor. The data also suggested that the inhibitor binds with higher affinity to the putrescine-binding site and only inhibits at higher concentrations when it saturates the active site. For *Pf*AdoMetDC, the inhibitor concentrations used were below 10 µM and no increase in activity was observed, which was expected since the putrescine-binding site is absent and is replaced with analogous positively-charged residues. This result shows that both the substrate and inhibitor can either fit within the active site, which suggests that the active site is large enough to accommodate both or that another more complex kinetic model is required. Alternatively the inhibitor might be binding at a site different from that of the active site, thus resulting in a negative allosteric effect. For *T. cruzi* the observed effect could be explained by the presence of Leu242, which, if mutated to the human counterpart (Thr), abolished inhibitor activation of activity and resulted in pronounced inhibition at lower inhibitor concentrations [186]. In *Pf*AdoMetDC this residue corresponds to Phe413, which is located adjacent to Phe415, an essential residue involved in substrate binding. Interestingly, human AdoMetDC inhibition with CGP48664 was shown to be extremely effective only in the presence of putrescine and subsequent co-crystallisation showed inhibitor binding within the active site [124].

Currently, AdoMetDC from various sources are classified into five distinct subclasses based on oligomeric structure (α- and β-subunits as well as prozyme binding), mechanism of autocatalytic processing and activation factors [196,197]. The subclasses can be divided into two main groups; those from bacterial or archeal origin are in Group 1 while the eukaryotic AdoMetDCs fall into the second group (Table 3.10). Group 1 is further subdivided based on oligomeric status and the requirement of a metal ion for activity (subclass 1a: gram-negative bacteria, tetramer) or an unknown activation factor (subclass 1b: gram-positive bacteria and archaea, dimer). Group 2 constitutes the eukaryotic enzymes that are not affected by putrescine (subclass 2a: plant, monomer) and those that do bind putrescine are further subdivided into the human (subclass 2b-I, dimer) and the trypanosomatids (subclass 2b-II, heterodimer with prozyme) AdoMetDC classes [196]. Based on these different groupings and with respect to monofunctional activity and oligomeric arrangement, *Pf*AdoMetDC seems to belong to the parasitic AdoMetDC subclass 2b-II. However, properties such as the unique bifunctional arrangement, the presence of parasite-

specific inserts and lack of activation by putrescine or prozyme denote that AdoMetDC from *Plasmodium* spp does not fall within the subclasses that are currently described. We therefore propose a distinct subclass for plasmodial AdoMetDCs, namely subclass 2b-III for which a possible activation factor remains to be indentified (Table 3.10).

Table 3.10: Subclasses of AdoMetDCs from different organisms

Subclass	Fold	Oligomer	Stimulation/activation	Organism
1a	$(\alpha\beta)_4$	Tetramer	Metal ion	*E. coli*
1b	$(\alpha\beta)_2$	Dimer	Unknown	*T. maritima*
2a	αβ	Monomer	None	*S. tuberosum*
2b-I	$(\alpha\beta)_2$	Dimer	Putrescine	*H. sapiens*
2b-II	αβ+prozyme	Heterodimer	Putrescine and prozyme	*T. cruzi, T. brucei*
2b-III	$(\alpha\beta)_2$+*Pf*ODC	Heterotetramer	*Pf*ODC?	*P. falciparum*

3.5. Conclusion

In conclusion, this study has shown that *Pf*AdoMetDC expressed from a codon-harmonised gene appears as a monomer in moderate protein concentrations but we have strong indications that at high concentrations an oligomer appears that corresponds to that of the human protein, an $(\alpha\beta)_2$ dimer. This dimer was also shown to be stabilised under oxidising conditions by the formation of a disulphide bond between the Cys505 residues from each monomer. *Pf*AdoMetDC has therefore not lost its ability to dimerise and shares quaternary structure similarities to that of human AdoMetDC. Nevertheless the dimer affinity of *Pf*AdoMetDC is orders of magnitude lower than the human orthologue. The results also showed that, according to the estimated K_d values and at the concentration used for determining the specific activity of *Pf*AdoMetDC, more than 95% of the protein exists in the (αβ) monomeric form. This correlates with a suggestion made previously that putrescine binding and dimerisation is linked [185]. Kinetics here and elsewhere [71] showed that monofunctional, monomeric *Pf*AdoMetDC behaves like other parasite AdoMetDCs while the bifunctional complex causes changes in the kinetic properties, which might be due to interdomain protein interactions imposed by the *Pf*ODC domain that result in coordinated domain activities. The results also show that an allosteric regulator remains to be identified that can activate the *in vitro Pf*AdoMetDC to the levels observed with the trypanosomal AdoMetDC and prozyme interaction [164,213]. Allosteric binding could induce conformational changes in one domain of the bifunctional complex that are then transmitted to the neighbouring domain. In our experiments *Pf*ODC seems the most likely target for such an effect as this domain is more refractory to change [69,103].

These studies contribute to the structural and functional characterisation of *Pf*AdoMetDC, which points towards the classification of this protein into a distinct structural class, suggested as 2b-III. Furthermore, this study has provided important starting points for crystallography from which the structure can aid in the identification of drug-like lead compounds for the inhibition of *Pf*AdoMetDC activity.